Journal of Alloys and Compounds 990 (2024) 174348

Contents lists available at ScienceDirect

Journal of Alloys and Compounds

journal homepage: www.elsevier.com/locate/jalcom

Linearization and characterization of the Wemple – DiDomenico model of ZnO/Ni/ZnO tri-layer thin films prepared by ALD and DC magnetron sputtering

S.S. Fouad [a], E. Barádacs [b,c], M. Nabil [d,*], A. Sharma [e], N. Mehta [e,*], Z. Erdélyi [c]

[a] Department of Physics, Faculty of Education, Ain Shams University, Cairo 11566, Egypt
[b] Department of Environmental Physics, Faculty of Science and Technology, University of Debrecen, Poroszlay u.6, Debrecen 4026, Hungary
[c] Departement of Solid-state Physics, Faculty of Science and Technology, University of Debrecen, P.O. Box 400, Debrecen 4002, Hungary
[d] Department of Basic Engineering Sciences, Faculty of Engineering (Shoubra), Benha University, Benha, Egypt
[e] Department of Physics, School of Physical Sciences, Mahatma Gandhi Central University, Motihari 845401, India

ARTICLE INFO

Keywords:
ZnO/Ni/ZnO films
ALD and DC evaporation techniques
Optical properties
Wemple-DiDomenico model
Nonlinear optical studies

ABSTRACT

Our present work is devoted to analyzing the influence of Ni on the optical properties of ZnO thin films deposited on glass and Si (100) substrates, with the use of ALD for ZnO deposition and DC magnetron sputtering for Ni interlayer deposition. The compositions as well as the crystalline structure of various multilayer thicknesses of Ni (10, 30, 50, and 70 nm), that sandwiched between ZnO Films (70 nm), before being optically characterized, were carried out by the X-ray diffraction (XRD). Based on the XRD results, the crystallite size was increased with the increase of the Ni interlayer concentration. Additionally, the material densities for both ZnO and Ni show the expected close-to-bulk values in all formations, where the large cavities between atoms, on the films make the dislocation density become smaller and the surface roughness values decrease as well, with the increase of Ni interlayer concentration. Different optical properties were observed for different Ni content. The optical absorption coefficient (α), refractive index (n), and extinction coefficient (k) have been deduced from the transmission T(λ) and absorption measurements A(λ). The optical energy gap E_g^{opt} are estimated from Tauc´s extrapolation procedure and the Kubelka-Munk approach. The static refractive index (n_o), the oscillator energy (E_o), and the dispersion energy (E_d) are calculated using the Wemple-DiDomenico (WDD) theoretical model. Analysis of third-order nonlinear optical properties in crystalline ZnO/Ni/ZnO are being detailed. These promising results imply that the high-quality films produced by ALD, show how the insertion of Ni could enhance the quality of the optical properties of ZnO films.

1. Introduction

Recently, the use of zinc oxide (ZnO), has increased because of its scientific importance and unique properties in electronic and optoelectronic devices, gas sensors, and several applications. It is a transparent conducting semiconductor oxide film providing a wide and direct band gap ($E_g = 3.2$ eV), and large exciton binding energy (~ 60 meV) at room temperature. ZnO is inexpensive with controllable electrical and optical properties, and environmentally friendly [1–3]. ZnO has higher photocatalytic efficiency under UV irradiation and lower photocatalytic activity in the visible region. Therefore, significant efforts have been made to increase the ZnO activity and improve the electrical and optical properties [4–6].

When we use ZnO in the thin-film version, its applications are expanded in a wide range of fields due to their unique properties [4–6] as shown in the flow chart of Fig. 1**(a)**. Thin films of ZnO doped with suitable elements are found useful in the fabrication of solid-state devices (e.g., solar cells, light emitting diodes (LEDs), gas sensors, varistors, piezoelectric devices, UV filters, etc.).

Zinc oxide (ZnO) thin films doped with metals can offer various benefits and alter the properties of the material for specific applications. The optical properties of ZnO thin films can be affected by metal doping and it may lead to changes in the bandgap, absorption, and emission characteristics. This is particularly useful in applications such as optoelectronic devices, sensors, and light-emitting diodes (LEDs). Doped ZnO thin films are often employed in photocatalysis for environmental

* Corresponding authors.
E-mail addresses: mohammed_diab35@yahoo.com (M. Nabil), drnmehta@bhu.ac.in, dr_neeraj_mehta@yahoo.co.in (N. Mehta).

https://doi.org/10.1016/j.jallcom.2024.174348
Received 5 January 2024; Received in revised form 28 March 2024; Accepted 29 March 2024
Available online 1 April 2024

remediation and solar energy conversion. Metal doping can improve the photocatalytic activity of ZnO by facilitating efficient charge separation and enhancing the material's performance in harnessing light energy [6]. Thus, the doping ZnO film with metals, such as Cu, Co, and Fe, is a common method to control some physical properties for desired applications [7–9]. Recent results indicate that Nickel has an important influence on enhancing the optical properties of ZnO [10–12]. These results also revealed that the physical properties of zinc oxide (ZnO) thin films can be significantly influenced by the preparation methods employed during their fabrication. Different techniques can result in variations in film structure, morphology, crystallinity, and other physical characteristics. For this purpose, the preparation method of ZnO films becomes important to control these properties. In this work, we have studied the influence of the Ni layer sandwiched between ZnO layers, on the crystalline structure and optical properties of ZnO/Ni/ZnO multilayer films grown on glass and Si(100) substrates.

2. Experimental procedures

ZnO has been prepared in Beneq TES-200–186 ALD system with a

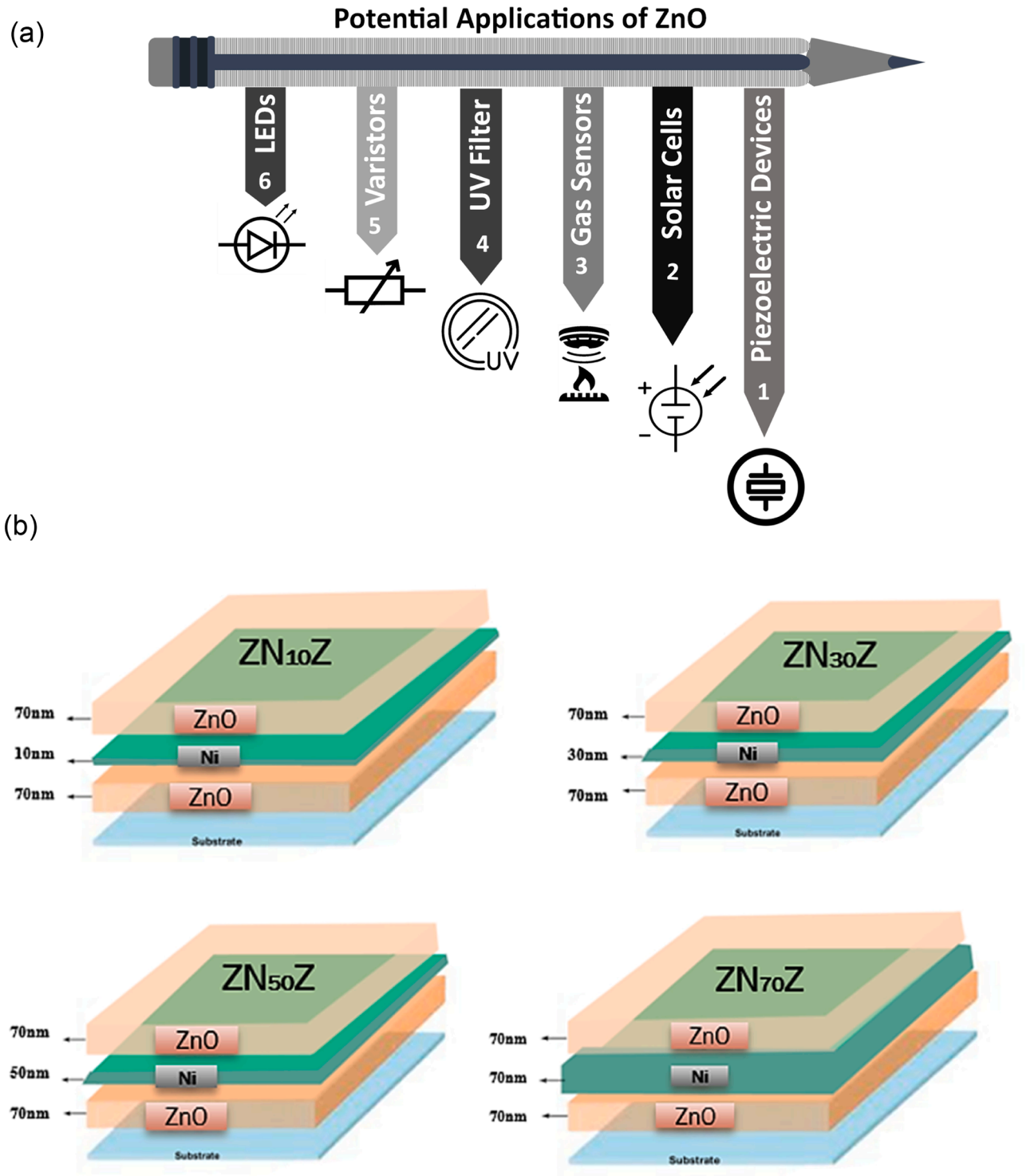

Fig. 1. **(a)**: Schematic presentation of some potential applications of ZnO. **(b)**: Schematic presentation of different multilayer ZnO/Ni/ZnO with sandwich structure.

nominal thickness of 70 nm on glass and Si(100) substrates with (25 × 25) mm and (10) mm sample size respectively, deposited at 200 °C in thermal mode in 391cycles. The pulse time and purge time were 0.3 and 3 seconds respectively for both diethylzinc (DEZ) and H_2O precursors. The MFC-NOP (mass flow controller for carrier gas and inert gas valving) and MFC-NOV (mass flow controller for vacuum chamber flow) parameters of nitrogen gas inlets for ZnO were: 300 and 300 sccm equally. Considering the sputtered Ni interlayers, the base pressure preceding the sputtering reached $P_{base} = 4 \times 10^{-7} mbar$ in each case. Interlayers with 10, 30, 50, and 70 nm nominal thickness were prepared at $P_{Ar} = 6 \times 10^{-3} mbar$ under high purity dynamic argon atmosphere. The deposition parameters were kept at $I = 150mA$, $U = 300V$, $P = 45W$, in a current controlled manner. Before the Ni depositions, the high-purity target was pre-sputtered for 2 minutes in each case to remove the surface contaminations from the target. The sputtering times for the 4 individual Ni interlayers were 68 s, 204 s, 340 s, and 476 s for the 10, 30, 50 and 70 nm thick Ni layers respectively. For the XRD analysis, we used a Rigaku Smart lab 9 kW X-Ray diffractometer. The measurements were performed in XRR (X-ray reflectometry) and GIXRD, also known as GID (Grain incidence x-ray diffraction) mode with a rotating Cu anode (λ = 0, 154 nm). The range of interest and step size were chosen to be 2θ = 0.6–1.2 (XRR) and 25–100° (GIXRD) and 0.05° respectively. The thickness of the ZnO layers was measured with a variable angle spectroscopic ellipsometer (Semilab SE-2000), and the thickness of the Ni layer with a profilometer (AMBIOS XP-1). In addition, thickness data were also determined from fitting XRR patterns. The different methods showed a very good agreement. The optical absorbance and transmittance measurements were recorded using a double-beam spectrophotometer (UV-3101PC Shimadzu) in the wavelength range of 300–700 nm. The schematic diagram of the prepared ZnO/Ni/ZnO thin films with different ratios of Ni is shown in Fig. 1**(b)**.

3. Results and discussion

3.1. Structural modification

The XRD patterns for the four thin film samples with different thick Ni layers sandwiched between the upper and lower layer of ZnO (70 nm), in the range 2θ =30° – 100° are shown in Fig. 2. The obtained XRD patterns clearly show distinguishable ZnO, Ni, and NiO peaks for each sample type. Also, the plotting of the normalized and fitted XRR patterns for the four deposited samples is given in Fig. 3.

The material densities for both the ZnO and Ni show the expected close-to-bulk values in all the different formations of the ZnO/Ni/ZnO system. The layer thicknesses are close to the nominal values of ZnO (70 nm)–Ni (70, 50, 30, 10 nm) –ZnO (70 nm) (**see** Table 1). The roughness values on the surface and between layers are small, so their uncertainty is relatively larger than that of the layer thickness values. The average crystallite size (D) of the four prepared samples was determined by Scherrer´s formula increments. The above-mentioned parameters are listed in Table 1. The dislocation density δ was measured by the following equation:

$$\delta = \frac{1}{D^2} \tag{1}$$

The values of the dislocation density (δ) decreases as the Ni thickness increases, which is accompanied by an increase in the grain size (D) as shown in Table 1.

These comparative results revealed the unique relationship between the deformation grain size and dislocation density and that the crystallization approach is perfect for increasing the film thickness by increasing the Ni concentration. This returns to the decrease in the interspacing between film grains which reveals the formation of higher quality films. In other words, the above-determined results showed that the Ni concentration has a fundamental impact on the lattice growth of ZnO.

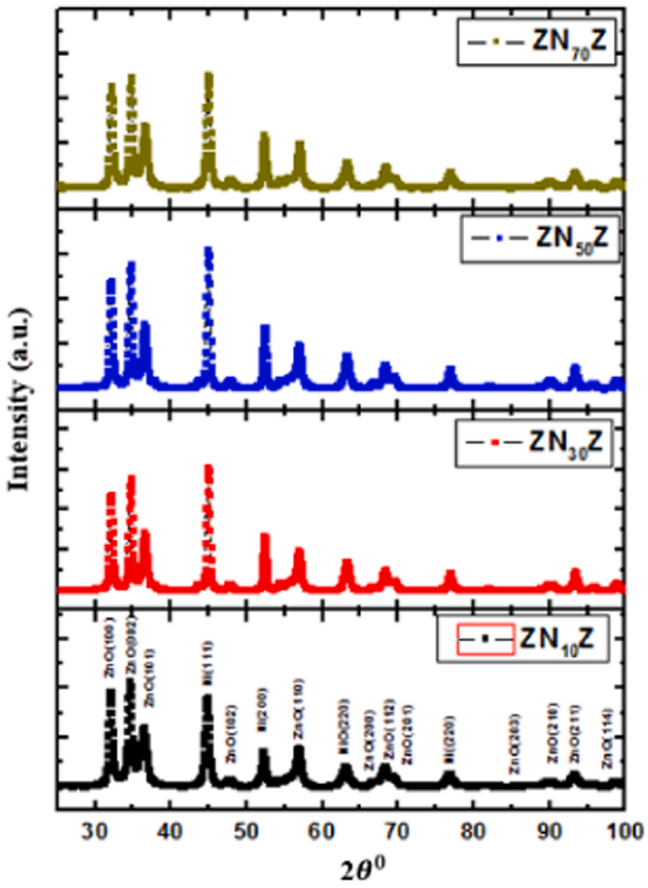

Fig. 2. : The XRD patterns of the four different samples of the ZnO/Ni/ZnO system.

3.2. Study of the spectral transmittance (T), reflectance (R), and absorbance (A)

Fig. 4(a-c) presents the transmittance, absorption, and reflectance spectra for $ZN_{10}Z$, $ZN_{30}Z$, $ZN_{50}Z$, and $NZ_{70}Z$. thin films. Fig. 4(a) shows a decreasing trend in the transmittance of the films with the increase in Ni concentration in ZnO/Ni/ZnO thin film samples. The observed transmittance peaks in the UV region (350–450 nm) diminished with the increase in the concentration of Ni. It is also reported that the optical transmittance of the four films from wavelength 550 nm is wavelength independent. Figs. 4(b) and 4(c) show the absorption and reflectance spectra of the four films under investigation, where both absorption and reflectance increased with the increase of thickness of interlayer Ni concentration, and they are almost independent of wavelength beyond 550 nm.

3.3. Computation and analysis of the absorption coefficient α and optical energy bandgap

The information about the optical energy band gap and structural arrangement of the materials can be revealed through the mechanism of absorption light. Its entire calculation mainly depends on the values of α. To determine the value of the absorption coefficient for ALD deposited tri-layers thin films of the ZNZ system in the region of the fundamental absorption edge, we utilized the measured results of transmittance spectra T (λ) in the strong absorption region and set in the following equation [13]:

$$\alpha = \frac{1}{d} \ln\left(\frac{1}{T}\right) \tag{2}$$

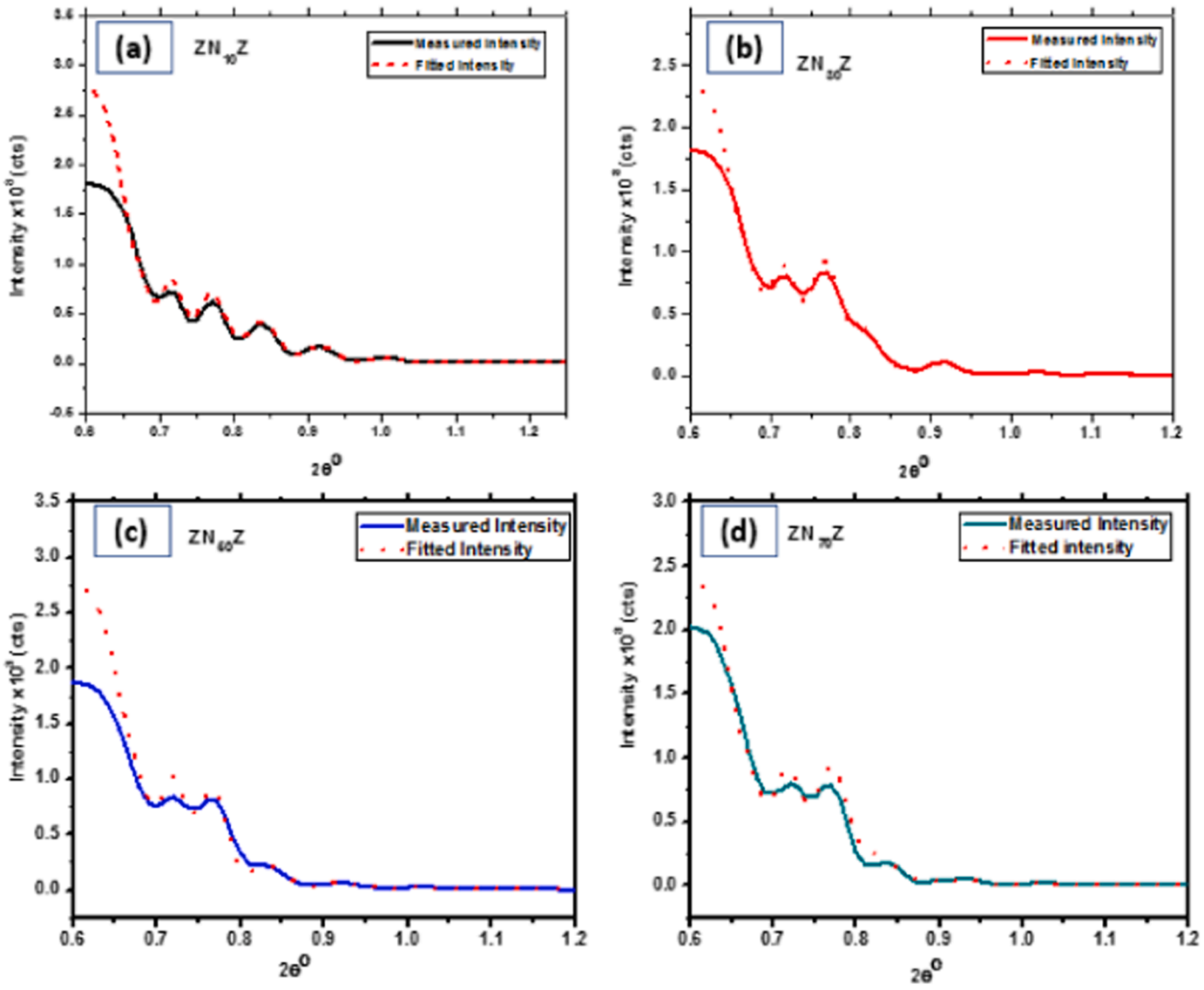

Fig. 3. : Fitted values and cumulative normalized residual plots of the four different samples of the ZnO/Ni/ZnO system.

Table 1
Calculated values of grain size, roughness, density, and dislocation density for ALD-deposited thin films of the ZnO/Ni/ZnO system.

Sample	Thickness (nm)		Grain Size (nm)	Roughness (nm)	Density (g/cm^3)	Dislocation density (nm^{-1})
	nominal	measured				
ZN10Z	150	145	8.03	3.192	5.6	0.124
ZN30Z	170	166	12.27	2.079	5.62	0.081
ZN50Z	190	185	12.87	1.891	5.67	0.077
ZN70Z	210	196	13.28	2.33	5.58	0.075

Here d is the thickness of the deposited thin film. The graphical illustration of α as a function of photon energy ($h\upsilon$) is depicted in Fig. 5 for all the deposited thin films. The figure shows that the optical absorption coefficient α decreases with increasing the energy and its value slightly increases with increasing thickness of interlayer Ni concentration.

The region where the value of absorption coefficient is greater or equal to 10^4 cm^{-1}, is ascribed as a Tauc's range, thereby, calculating the optical energy band gap, E_g^{opt} by using these absorption spectra [14] and set into the following relation:

$$\alpha h\nu = B\left[h\nu - E_g^{opt}\right]^y \tag{3}$$

Here, constant B measures the disorderness of the system and it is defined by the following equation:

$$B = 4\pi\sigma/n_0 c\Delta E \tag{4}$$

Here n_0 is the refractive index, σ is the conductivity, c is the speed of light, and ΔE is the band tailing. In Eq. (3) y is the transition parameter. The values of y are chosen through the kinds of transition corresponding to the absorption edge. The dissimilar values of y associated with different transitions are 0.5, 2, 1.5, and 3 respectively. These values

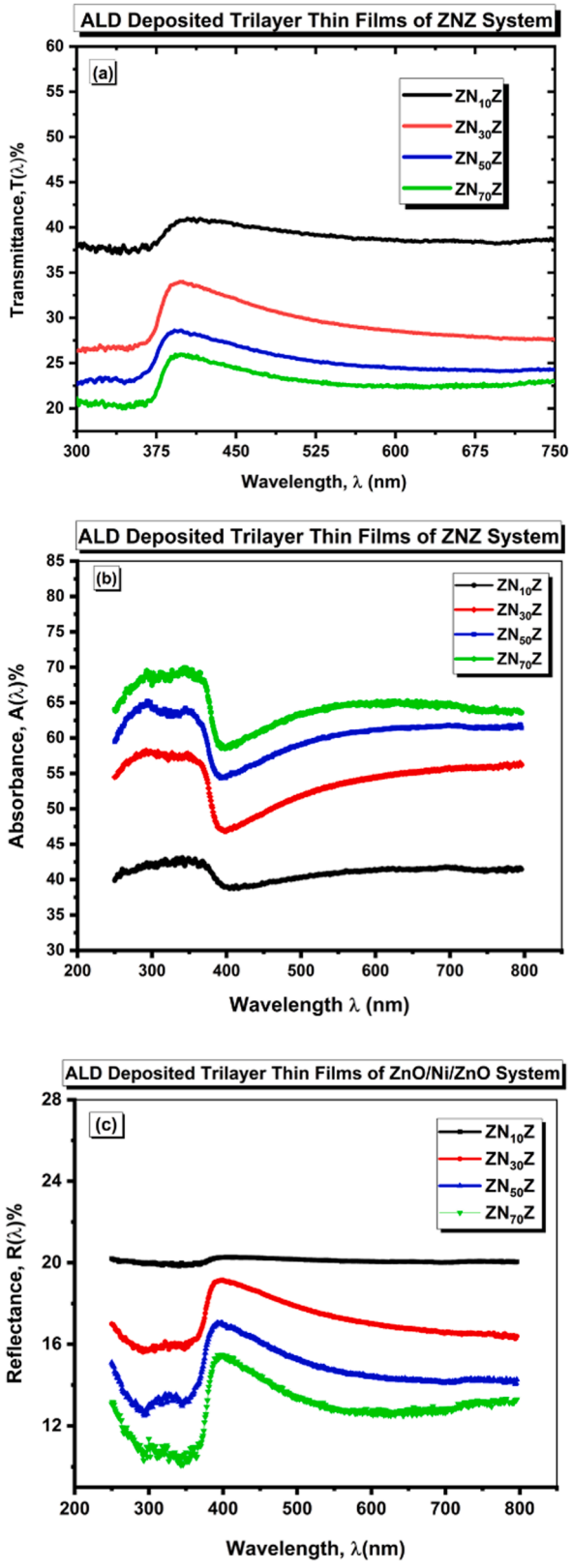

Fig. 4. (a): An illustration of transmittance spectra as a function of wavelength of incident radiation for the ALD deposited different multilayer thin films of the ZnO/Ni/ZnO system. **(b)** An illustration of absorbance spectra as a function of wavelength of incident radiation for the ALD deposited different multilayer thin films of the ZnO/Ni/ZnO system. **(c):** An illustration of reflectance spectra as a function of wavelength of incident radiation for the ALD deposited different multilayer thin films of the ZnO/Ni/ZnO system.

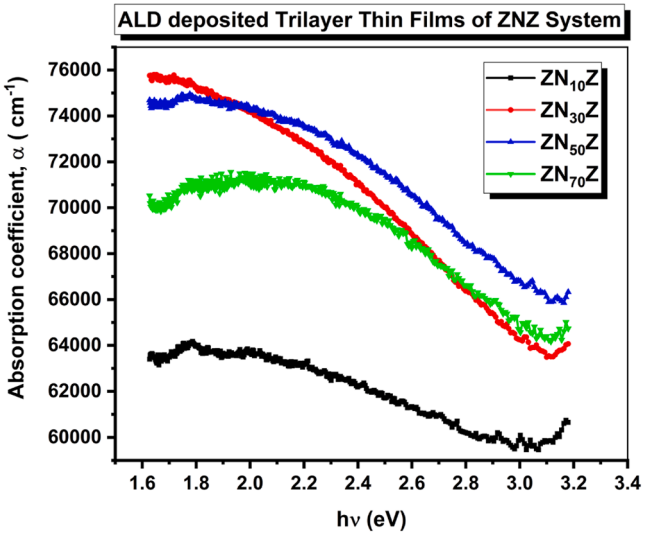

Fig. 5. : An illustration of absorption coefficient as a function of incident photon energy for ALD deposited different multilayer thin films of the ZnO/Ni/ZnO system.

correspond to the direct allowed, indirect allowed, direct forbidden, and indirect forbidden transitions [14]. A linear connection between $(\alpha h\nu)^2$ and $h\nu$ suggests that direct transition can take place for the proposed ALD-deposited thin film system. The values of the $E_{g(1)}^{opt}$ were computed from the linear portion of Tauc's plot which denotes the intercept on the $h\nu$ axis obtained by extrapolating the linear portion of the curves at $(\alpha h\upsilon)^2 = 0$ and are depicted in Fig. 6(a-d). These computed values of direct allowed bandgap $E_{g(1)}^{opt}$ after extrapolation from Tauc's plot for all ALD deposited thin film samples are highlighted in Table 2.

Moreover, to estimate the optical band gap of the proposed ALD deposited tri-layer thin films of the ZNZ system another approach of the Kubelka-Munk (K-M) model was utilized [15,16]. According to the model, a flux of radiation normal to the surface of the thin film sample is considered. To compute both K-M functions and reflectance, the measured value of reflectance optical spectra. The optical band gap is thus, estimated using the direct function given by the following equation:

$$[F(\alpha)h\nu]^2 = A\left(h\nu - E_g\right) \tag{5}$$

In this above equation, $F(\alpha)$ represents the K-M function. Computation of optical energy band gap $E_{g(2)}^{opt}$ is possible by plotting $[F(\alpha)h\nu]^2$ as a function of the energy of incident light $(h\nu)$. It is estimated through the extrapolation of the linear portion of the plot on the $h\nu$-axis, when K-M function $F(\alpha)$ has zero value associated with the photon energy of incident light [15]. A graphical representation of the K-M plot to estimate the optical band gap is shown in Fig. 7(a-d) for the present thin film system. The estimated optical band gap $E_{g(2)}^{opt}$ values for all the thin film samples are tabulated in Table 2. It has been observed that the values of optical band gap increase with increasing the Ni interlayer thickness sandwiched between ZnO thin film layers. There may be other causes for energy gap fluctuation like the variation in the film morphology. Generally, the increase of optical band gap in this work may be interpreted as the presence of unstructured defects, which subsequently increases the grain size as given in [17] and has been confirmed by the increase in the value of the grain size of the thin films under investigation, given in Table 1.

The plot of the optical band gap of Tri-layer thin films as a function of the monolayer thickness of the Nickle (Ni) constituent is shown in Fig. 8. This figure reveals that the large changes in thickness yield a large band gap change $\Delta E_{g(1)}^{opt} \approx 0.49$eV; from Ni-10 nm to Ni-50 nm thin films.

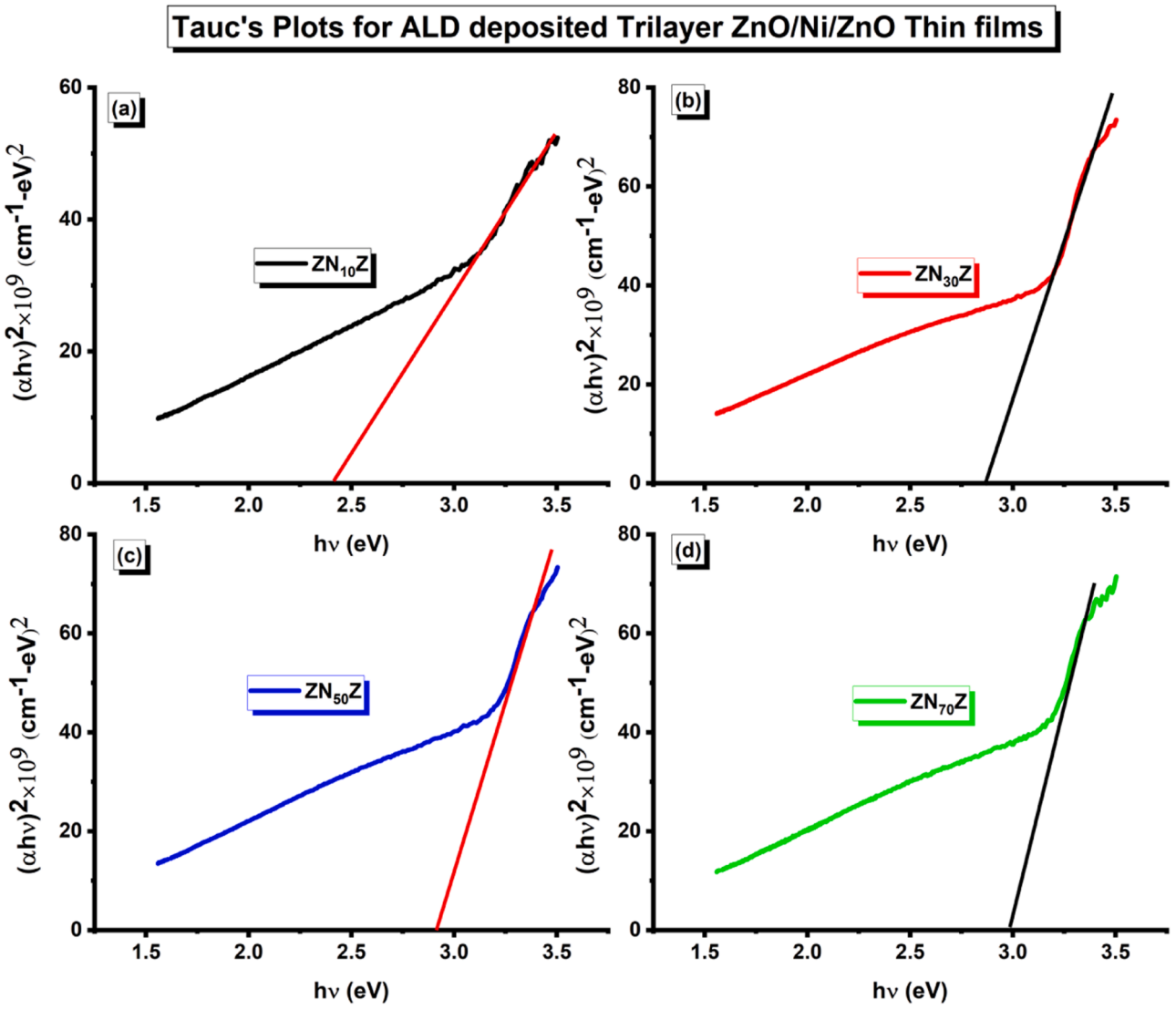

Fig. 6. (a-d): A graphical representation of Tauc's plots for the computation of optical energy band gap for ALD deposited different multilayer thin films of the ZnO/Ni/ZnO system.

Table 2
The computed values of optical band gap (E_{g1}^{opt} and E_{g2}^{opt}), optical constant B, metallization criterion M, electronic polarizability α_e, and refractive index (η_0) for the ALD deposited different multilayer thin films of the ZnO/Ni/ZnO system.

Sample	E_{g1}^{opt} (eV) (Tauc plot)	E_{g2}^{opt} (eV) (K-M plot)	B (cm-eV)$^{-1}$ (Tauc Plot)	B_1 (cm-eV)$^{-1}$ (Empirical fit)	y (Permitted direct Transition)	y (from Empirical Relation)	Metallization M	electronic polarizability $\alpha_e \times 10^{-24}$	η_0
$ZN_{10}Z$	2.46	2.06	2.24×10^5	2.22×10^5	0.50	0.50	0.347	9.34	2.58
$ZN_{30}Z$	2.86	2.97	5.84×10^5	3.54×10^5	0.50	~ 0.49	0.378	8.94	2.44
$ZN_{50}Z$	2.90	3.02	5.84×10^5	3.59×10^5	0.50	~ 0.47	0.381	8.90	2.42
$ZN_{70}Z$	2.99	3.17	5.84×10^5	3.79×10^5	0.50	~ 0.40	0.387	8.82	2.40

However, a small modification in the thickness of Ni from 50 nm to 70 nm, makes a quite small change in the gap difference of ≈ 0.09eV. Moreover, the variation in the optical bandgap with increasing the concentration and thickness of interlayer Ni material opens an opportunity for the modification and advancement of the chemical and physical properties of layered materials. Changing the concentration of interlayer Ni material in a triple-layer thin film system can affect the motion of charge carriers, or even cause structural modifications owing to the formation of localized levels in prohibited gaps [15]. Further, the computed values of optical band gap from two different kinds of

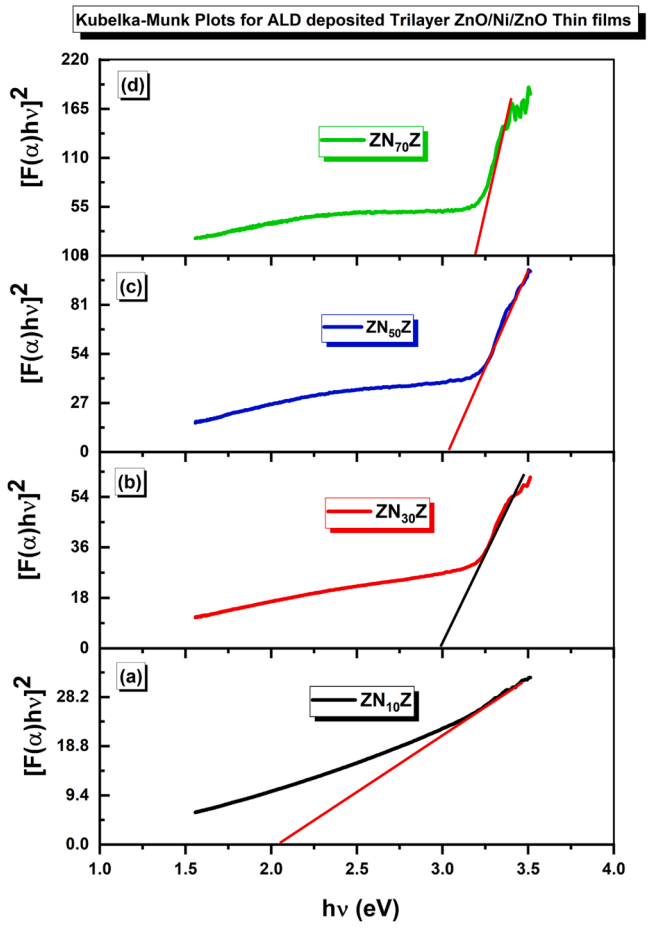

Fig. 7. (a-d): A graphical representation of Kubelka-Munk's plots for the computation of optical energy band gap for ALD deposited different multilayer thin films of the ZnO/Ni/ZnO system.

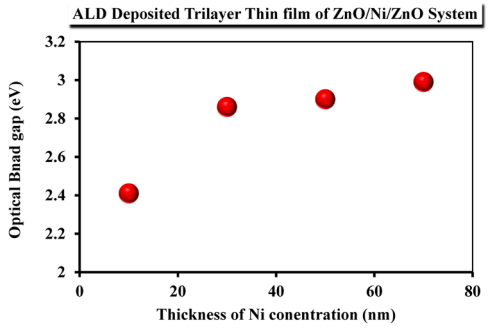

Fig. 8. : A graphical representation of the optical energy band gap against the inter-layer thickness of Ni concentration for ALD deposited different multilayer thin films of the ZnO/Ni/ZnO system.

approaches under the present work have shown closer results.

To validate the value of the power factor or transition parameter *y*, one can make an empirical relation [18] just by utilizing Tauc's formulation. It can be written by relating α and $h\upsilon$ as:

$$\alpha = \frac{B}{h\nu}\left[h\nu - E_g^{opt}\right]^{y} \tag{6}$$

Here constant B denotes different values associated with the different types of transitions and it is represented by the power factor y. Thus, the above equation can be stated for occurring four different types of transitions:

$$\alpha = \sum_{j}^{4} \frac{B_j}{h\nu}\left[h\nu - E_{g_j}^{opt}\right]^{y_j} \tag{7}$$

In this above equation, separate magnitudes of y_j in the sequence of 0.5, 2, 1.5, and 3 are for permitted direct, permitted nondirect, forbidden direct, and forbidden nondirect transitions, respectively. For the case of a material that has only direct permitted transition, the relation (7) can be defined by the updated form as:

$$\alpha = \frac{B_1}{h\nu}\left[h\nu - E_{g_1}^{opt}\right]^{y_1} \tag{8}$$

By simply taking the natural logarithm of the relation (8) and validating the result of transition factor y_1 for a single allowed direct transition, we obtain:

$$\ln(\alpha h\nu) = \ln B_1 + y_1 \ln\left(h\nu - E_{g_1}^{opt}\right) \tag{9}$$

For the present case, the values of the direct permitted band gap, $E_{g(1)}^{opt}$ for all the samples are already computed from the Tauc's plot, thus, y_1 can be determined through the slope of the linear fitted plot between $ln(\alpha h\nu)$ and $ln(h\nu - E_{g_1(1)}^{opt})$ by using the relation (9). An illustration of a such linear fitting is depicted in Fig. 9(a-d). From the linear plot, the value of the transition factor, y_1 is determined from the slope, and it is close ~ 0.5 for each sample under the present study. The determined result of the transition factor (y_1) supports that, the transition is band to band allowed in ALD deposited all layered thin film samples of ZNZ as mentioned in the Fig. 6(a-d). In addition, the values of y_1 for assorted deposited thin film samples are publicized in Table 2.

3.4. Computation of the linear index of refraction (n) and the extinction index (k)

The index of refraction, n is a substantial parameter that defines an exclusive feature of any substance. This unique feature plays an important role in deciding which materials are suitable for designing different optical applications. Also, the refractive index (n) affects various optical phenomena, which makes its valuation decisive, as it has a vast impression on both the local field inside the optical materials along the electronic polarization of ions [19]. To calculate the values of the refractive index of the ZN10Z, ZN30Z, ZN50Z, and ZN70Z thin films by using the reflection spectra, R(λ) from the given relation [20]:

$$n = \left[\frac{(1+R)^2}{(1-R)^2} + (1-k^2)\right]^{1/2} + \frac{(1+R)}{(1-R)} \tag{10}$$

In this equation, k represents to extinction coefficient, and it is defined by the following formula:

$$k = \frac{\alpha\lambda}{4\pi} \tag{11}$$

It is a very substantial parameter for determining corresponding optical properties, particularly those associated with the absorption of photon energy and optical dielectric parameters for the materials. Fig. 10(a-d) and Fig. 11(a-d) show the wavelength dependence of the refractive index n and extinction coefficient k rrespectively. The results disclose that the k values are increased with the rise increasing the wavelength of the incident radiation over a range of 400 – 790 nm for all the deposited multilayer thin films of the present system.

3.5. Metallization criterion

For the possibility of application to designing optical devices, information about the fundamental parameter linear index of refraction may be more important. Duffy suggested a formulation to compute the result of the linear index of refraction (n_0) with the help of the optical

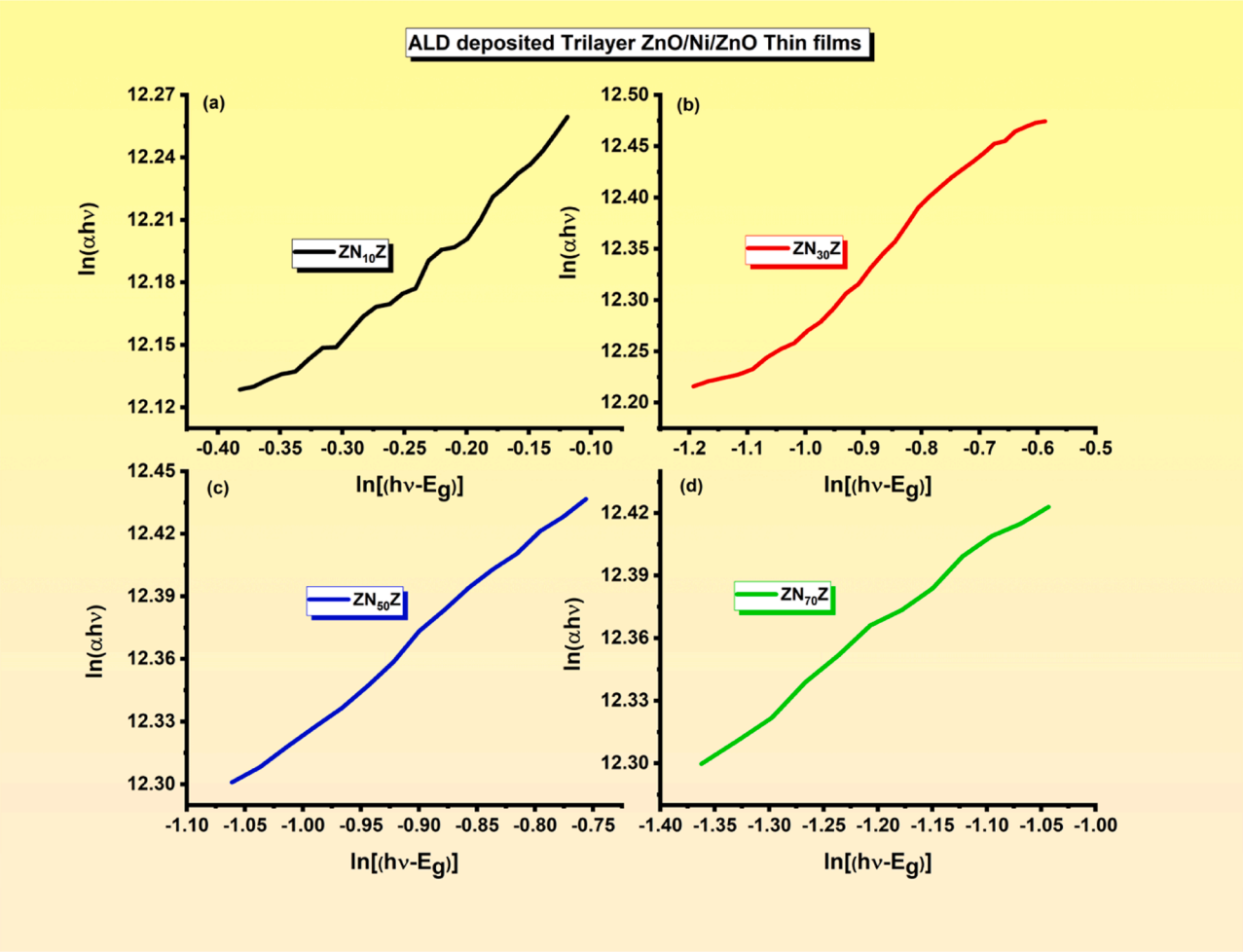

Fig. 9. (a-d): A graphical representation of ln(αh*ν*) against ln (hν E_g^{opt}) to approve the direct allowed transition in ALD deposited different multilayer thin films of the ZnO/Ni/ZnO system.

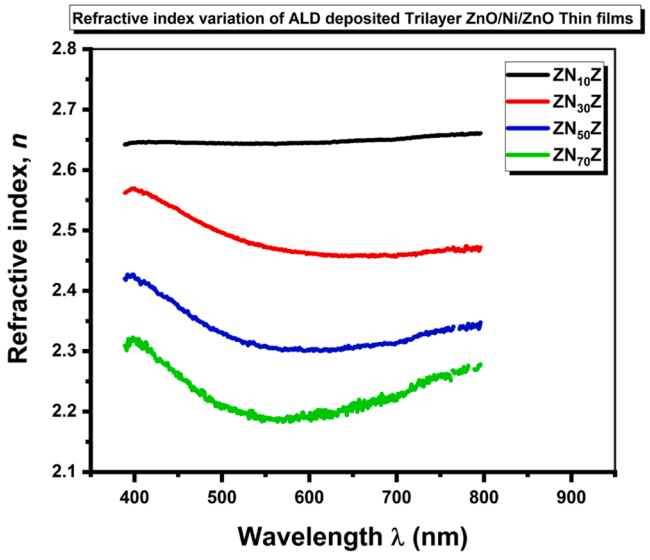

Fig. 10. : An illustration of refractive index as a function of wavelength of incident radiation for ALD deposited different multilayer thin films of the ZnO/Ni/ZnO system.

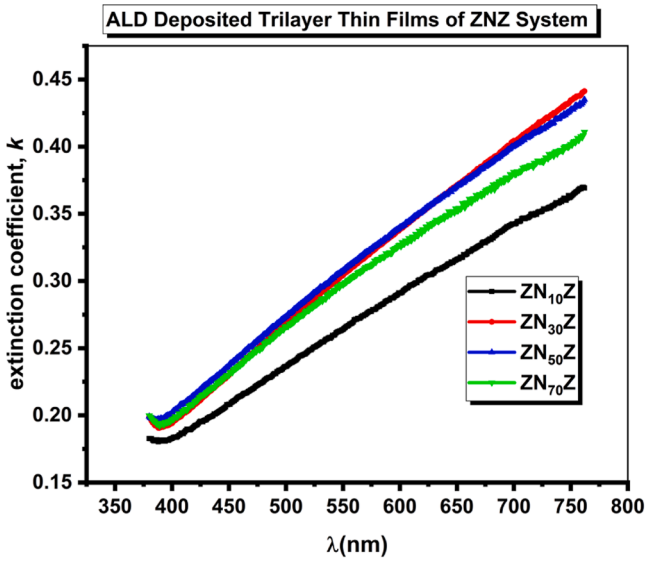

Fig. 11. : An illustration of extinction coefficient as a function of wavelength of incident radiation for ALD deposited tri-layer thin films of the ZnO/Ni/ZnO system.

energy gap E_g^{opt} over attempting the subsequent relation [21]:

$$\left(1-\frac{\eta_0^2-1}{\eta_0^2+2}\right)=\frac{1}{2}\sqrt{\frac{E_g^{opt}}{5}} \tag{12}$$

The computed value of the (η_0) for all the thin film samples is recorded in Table 2. The value of the refractive index (η_0) decreases with increasing the concentration of the internal layer of Ni and thickness in triple-layer thin film samples.

Moreover, the computation of the metallization criterion is a very important parameter in understanding the nonlinear optical characteristics of the yielded materials. It can be defined by the subsequent relation [22]:

$$m=\left(1-\frac{R_m}{V_m}\right) \tag{13}$$

The aforementioned form can be described based on Duffy's empirical relation that relates the energy gap to the metallization criterion m by the following relation [23]:

$$\left(1-\frac{R_m}{V_m}\right)=\frac{1}{2}\sqrt{\frac{E_g^{opt}}{5}} \tag{14}$$

Here V_m and R_m represent to molar volume and molar refraction of the envisioned system, respectively. According to the metallization criterion suggested by Herzfeld [24], for the case of $R_m/V_m = 1$, the linear index of refraction becomes infinite, which links to the metallization of covalent solid materials. Consequently, the necessary cases for making metallic or nonmetallic solids are $R_m/V_m \geq 1$ (for metal) or $R_m/V_m < 1$ (for nonmetal). The computed values of the metallization criterion (m) for the present deposited layer system are recorded in Table 2. It increases with increasing the interlayer thickness of Ni concentration from 10 to 70 nm in all the deposited multilayer thin films of the present system. This change shows that the present multilayer thin film behavior moves to a metallic to slight metallic nature with increasing the interlayer thickness of Ni. The changes can be seen from (0.347–0.387) for the metallization criterion depicts a smaller width in the valence band and conduction band, which causes an increase of the energy band gap from (2.46–2.99 eV). Thereby, it confirms an appropriate connection between the linear index of refraction η_0, energy gap $E_g^{opt}$and the metallization criterion M. These results can be a nice basis for envisaging novel nonlinear optical materials. The rise in the energy band gap could potentially result from the sp-d exchange interaction between localized d-electrons linked to doped Ni^{2+} cations and ZnO band electrons.

The sp-d hybridization occurs when Ni^{2+} ions are introduced to ZnO, resulting in the 3d levels of impurity Ni^{2+} ions existing below the conduction band of ZnO. Thus, an increase in sp-d hybridization energy may be the reason for the rise in the band gap energy of ZnO with increasing Ni concentration. Similar results were obtained by other research groups which indicates that our observations are consistent with available reports in the literature of recent years [25–29].

Pal et al. [25] performed the XPS analysis of Ni, ZnO and Ni-doped ZnO and observed that Ni ions are successfully substituted into tetrahedral sites of the ZnO wurtzite structure without forming any detectable secondary phases. Ni^{2+} ions have an electronic configuration of 3d8. When introduced into the ZnO lattice, the Ni^{2+} ions can interact with the surrounding oxygen and zinc ions. In the process, the electrons in the d orbitals of Ni^{2+} can participate in bonding with the electrons from the oxygen and zinc ions. In the ZnO lattice, zinc ions typically contribute s electrons, while oxygen ions contribute p electrons for bonding. When Ni^{2+} ions are introduced, there can be an overlap between the d orbitals of Ni^{2+} and the s and p orbitals of Zn and O, respectively. This overlap allows for the formation of sp-d hybrid orbitals. Srinet et al. [27] also observed the signature of strong hybridization of Ni in ZnO host matrix. They observed that the occurrence of sp-d hybridization can modify the electronic band structure of ZnO. It can lead to changes in the energy levels and band gaps, as well as affect the bonding strength and electronic properties of the material. These changes can manifest as alterations in the optical, electrical, and magnetic properties of Ni-doped ZnO.

The study of polarization for different thin film systems is decisive due to the necessity to design efficient materials for optical purposes along with a high optical performance of these materials. A well-known equation based on the polarizability approach is the Lorentz-Lorentz relation defined by the Eq. (13). According to the equation, the molar fraction (Rm) can be linked to the molar polarizability α_m through the linear relation $R_m = 2.52\alpha_m$. Briefly, the role of polarizability as a vital parameter of the linear index of refraction and optical band gap of the present work on different multilayer thin films of the ZnO/Ni/ZnO has been highlighted. The relationship presented a linear proportionality between the index of refraction and the polarizability, and this visibly shows the linear dependency of R_m on the polarizability. Electronic polarizability (α_e) plays a significant role in designing optical functional materials such as oxides. It is closely connected to the field of optics and is a noteworthy distinctive feature of any substance. It was observed that the non-linearity response of the substance is directed by the electronic polarizability parameter (α_e). It can be computed in terms of the linear index of refraction from the subsequent relation [30]:

$$\alpha_e=\frac{3}{4\pi N_A}\frac{\left(n_0^2-1\right)}{\left(n_0^2+2\right)} \tag{15}$$

Here N_A represents Avogadro's number. The computed values of α_e under the present study, all the thin film samples are recorded in Table 2. The computed results revealed that the linear refractive index and the energy gap, which are linked to polarizability and the oxides metallicity of the material, have a strong relationship with the increase of the thickness of the different multilayer thin films of the ZnO/Ni/ZnO system.

3.6. Computation and analysis of dispersion parameters E_d and E_o using the Wemple-DiDomenico (WDD) model

The spectral distribution of the index of refraction n in the normal dispersion for materials under the interband absorption side can be explored by using a single-effective oscillator model. This model is also recognized as a Wemple-DiDomenico (WDD) model [31,32] and is mainly based on the change in dielectric constant as a function of spectral frequency because of the concept of a single oscillator in terms of energy of a single oscillator represented by E_o and dispersion energy by E_d. Accordingly, the WDD model is utilized by fitting the data of dispersion in the index of refraction for the yielded system. Information about the dispersion in the optical material can be an important aspect in many areas of scientific research that supports to design of devices for optical communication and spectral dispersion. In this supposed model, the relation of the index of refraction, n with E_o and E_d is represented by the following expression [31,32]:

$$n^2-1=\frac{E_0E_d}{{E_0}^2-(h\nu)^2} \tag{16a}$$

The above equation can be redrafted in another way as:

$$\frac{1}{(n^2-1)}=\frac{{E_0}^2-(h\nu)^2}{E_0E_d}=\frac{E_0}{E_d}-\frac{(h\nu)^2}{E_0E_d} \tag{16b}$$

The experimental validation of equation (16) can be realized by plotting the data of $(n^2-1)^{-1}$ as a function of $(h\nu)^2$ (see Fig. 12). The linear behaviour of the curve shown in Fig. 12 validates the applicability of this relation. To determine the values of E_d and E_o for the present study, we solve simultaneously two different equations received through the slope $[1/(E_0E_d)]$ and vertical intercept $[E_0/E_d]$ of the aforesaid linear plots. The computed values of the energy dispersion parameters E_d and E_o for deposited all thin film are recorded in Table 3. Additionally, to

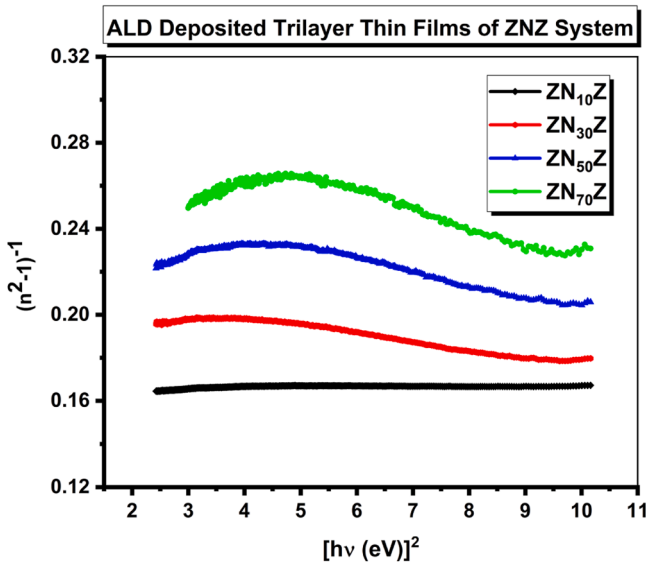

Fig. 12. : A graphical representation of $(n^2\text{-}1)^{-1}$ against $(h\nu)^2$ for ALD deposited different multilayer thin films of the ZnO/Ni/ZnO system.

compute the value of the dielectric constant at low frequency ($\nu = 0$) or high wavelength ($\lambda = \infty$) side as defined by $\varepsilon_{\infty}^{WDD} = n_0^2$, the value of n_0 in such a limit $h\nu \to 0$ is determined through the dispersion relation [i.e., $n_0 = \sqrt{1 + E_d/E_o}$]. The probable computed values of $\varepsilon_{\infty}^{WDD}$ and static index of refraction for the present thin film samples are mentioned in Table 3. We can see from Table 3 that all the computed WDD parameters are decreased with changing the thickness of inter-atomic Ni concentration from 10 to 70 nm in the case of all the deposited thin film samples. The results of all WDD parameters for the projected multilayer thin films of the ZNZ system are consistent with those of other systems stated elsewhere [33].

Furthermore, the WDD model establishes simple connections among the dispersion parameters E_o, E_d, and the imaginary portion of the dielectric constant ε'' for the values of moments M_{-3} and M_{-1} of the optical spectrum [32]. The following relations are used to compute the values of M_{-1} and M_{-3} [32]:

$$E_0^2 = \frac{M_{-1}}{M_{-3}} \tag{17a}$$

$$E_d^2 = \frac{M_{-1}^3}{M_{-3}} \tag{17b}$$

The computed values of moments M_{-1} and M_{-3} for all the samples are listed in Table 3.

3.7. Determination and analysis of optical dispersion parameters using the Sellmeier model

To obtain the optical dispersion parameters a classical dispersion relation for the single oscillator model was established by Sellmeier for low frequencies, which is given by the subsequent equation [34]:

$$\left[\frac{n_0^2 - 1}{n^2 - 1}\right] = 1 - \left(\frac{\lambda_0}{\lambda}\right)^2 \tag{18}$$

Simplifying above equation, we obtain:

$$\frac{1}{n^2 - 1} = \frac{1}{(n_0^2 - 1)} - \frac{1}{(n_0^2 - 1)}\left(\frac{\lambda_0}{\lambda}\right)^2 \tag{19a}$$

Using the well-known Planck's relation $c = \lambda\nu$, the Eq. (19a) becomes:

$$\left(\frac{1}{n^2 - 1}\right) = \frac{1}{(n_0^2 - 1)} - \frac{1}{(n_0^2 - 1)}\lambda_0^2 \quad \left(\frac{h\nu}{hc}\right)^2 \tag{19b}$$

On comparison of two Eqs. (12) and (19b), therefore, we obtain:

$$\frac{1}{n_0^2 - 1} = \frac{E_0}{E_d} \tag{20a}$$

$$\text{and} \frac{1}{(n_0^2 - 1)}\lambda_0^2\left(\frac{1}{hc}\right)^2 = \frac{1}{E_0 E_d} \tag{20b}$$

Simultaneously simplifying Eqs. (20a) and (20b), we get the following solutions for the oscillator's strength (S_o) and the oscillator wavelength (λ_o):

$$(n_0^2 - 1)\frac{hc}{\lambda_0} = E_d \text{and} \lambda_0 = \frac{hc}{\mathrm{E}_0} \tag{21a}$$

$$\frac{(n_0^2 - 1)}{{\lambda_0}^2} = S_0 \tag{21b}$$

Therefore, by setting the values of E_o and E_d, already determined from the WDD model, we can obtain the values of λ_o and S_o. Thus, the calculated values of Sellmeier parameters viz. λ_o, S_o, and E_o/S_o for the present work are tabulated in Table 3. In the subsequent approach, the calculated results of the Sellmeier parameters can also have been defined through a graphical depiction subsequently reformulating the Eq. (14) in this way [35]:

$$\left[n^2 - 1\right]^{-1} = \frac{1}{\lambda_0^2 S_0} - \frac{1}{S_0 \lambda^2} \tag{22}$$

To get the Sellmeier parameters viz. λ_o, S_o, and E_o/S_o, through a graphical illustration, we plot the connection between the two variable results; as the reciprocal of $[n^2 - 1]$ with $1/\lambda^2$; we obtain a straight linear plot having a gradient $(1/S_0)$, and the intercept on the vertical axis is $(1/\lambda_0^2 S_0)$. Consequently, the value of S_o can be computed through the gradient of the plot, whilst the oscillator wavelength λ_o is defined by using the gradient and intercept. A linear graphical relationship between $[n^2 - 1]^{-1}$ and $1/\lambda^2$ for the proposed work are represented in Fig. 13. Moreover, the calculated values of Sellmeier parameters for ALD-deposited tri-layer thin films of ZNZ samples are highlighted in Table 3.

3.8. Nonlinear Optical Studies

The nonlinear optical parameters of materials can be described by the response of the polarization vector when incident radiation crosses over it. The polarizability shows a highly dependent result on the

Table 3
The calculated values of WDD and Sellmeir parameters for the ALD deposited different multilayer thin films of the ZnO/Ni/ZnO system.

Sample	WDD Parameters						Sellmeir Parameters			
	E_d (eV)	E_o (eV)	n_0	$\varepsilon_{\infty}^{WDD}$	M_{-1}	M_{-3} $(eV)^{-2}$	λ_0 (nm)	$(\varepsilon_{\infty})_1$	S_o (m^{-2})	E_o/S_o $(eV\text{-}m^2)$
$ZN_{10}Z$	174	28.73	2.66	7.06	6.06	0.007	69	7.06	1.26×10^{15}	2.27×10^{-14}
$ZN_{30}Z$	41.53	8.60	2.41	5.83	4.83	0.065	231	5.83	9.03×10^{13}	9.53×10^{-14}
$ZN_{50}Z$	37.91	9.10	2.27	5.17	4.17	0.050	219	5.17	8.72×10^{13}	1.04×10^{-13}
$ZN_{70}Z$	29.31	8.12	2.15	4.61	3.61	0.055	245	4.62	6.02×10^{13}	1.35×10^{-13}

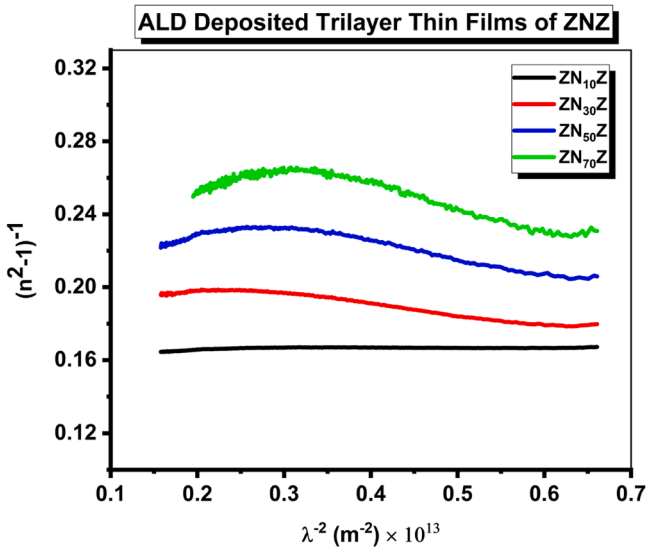

Fig. 13. : A graphical representation of $(n^2 - 1)^{-1}$ against λ^{-2} for ALD deposited different multilayer thin films of the ZnO/Ni/ZnO system.

dielectric parameter as an intrinsic property of the dielectric materials and is regulated by its n and k values. As we know the nonlinear character of substances is directly linked to their index of refraction values, thus, the changes in the host structure were noticed owing to the inclusion of foreign chemical species. This may be the reason for a resulting variation in the optical susceptibility of the substance. Technological applications point of view, the susceptibility of materials must have good nonlinearity, especially for designing nonlinear optical devices along with integrated photonics, infrared sensing, and all-optical switching. Consequently, to explore the feasibility of the materials for optoelectronic applications, the study of nonlinear optical properties is important [36]. We can see that there exists a resulting power series expansion of polarization, $\vec{P}$ of a dielectric material in terms of and susceptibility parameter (χ) and the electric field vector $\vec{E}$ [37]:

$$\vec{P} = \epsilon_0\left[\ \chi^{(1)}.\vec{E} + \chi^{(2)}.\vec{E}^2 + \chi^{(3)}.\vec{E}^3 + \ldots\right] \tag{23}$$

where $\chi^{(1)}$ represents the first-order linear susceptibility which shows the linearization of the polarization terms of n_0. In the Eq. (22), the term $\chi^{(2)}$ is represented by the second-order susceptibility. It has non-zero values for those substances which show the absence of inversion symmetry, on the other hand, its value becomes zero for radially symmetrical materials.

By the application of calculated values of E_o and E_d from the WDD method and the general Miller's relation in the limiting condition of $h\nu \to 0$, the estimation of third-order-nonlinear optical susceptibility, $\chi^{(3)}$ is defined by the ensuing relation [38]:

$$\chi^{(3)}(esu) = \frac{F}{(4\pi)^4}\left[n_0^2 - 1\right]^4 \tag{24a}$$

$$\chi^{(1)} = \frac{1}{4\pi}\left[n_0^2 - 1\right] \tag{24b}$$

As earlier defined the form- $\left[n_0^2 - 1\right] = \frac{E_d}{E_0}$ in the limit of $h\nu \to 0$ Thereby,

$$\chi^{(1)} = \frac{1}{4\pi}\left[\frac{E_d}{E_0}\right] \tag{24c}$$

Here F represents a constant, the value of the constant is equal to 1.7 $\times$ 10^{-10} (esu) and it is free from the periodic nature of the materials along with the photon energy. Using the preceding equations, the aforementioned relation is thus, transformed in terms of energy oscillator parameters E_o and E_d:

$$\chi^{(3)}(esu) = \frac{F}{(4\pi)^4}\left[\frac{E_d}{E_0}\right]^4 = 6.82 \times 10^{-15}\left[\frac{E_d}{E_0}\right]^4 \tag{24d}$$

Therefore, all the results associated with the nonlinear optical parameters for the present work are estimated by using these equations. Additionally, the computation of n_2 (i.e., second-order nonlinear index of refraction) is also feasible either from the calculated value of the static index of refraction, $n_{0,}$ or from the obtained value of optical band-gap energy, E_g^{opt}, in the following equation proposed by Tichy and Ticha [38]:

$$n_2\left(esu(eV)^4\right) \cong 12\pi\frac{\chi^{(3)}}{n_0} \tag{24e}$$

Accordingly, the values of n_2 were computed by utilizing the above equation for the present ALD deposited tri-layer thin film samples. All the calculated values of $\chi^{(1)}$, $\chi^{(3)}$, and n_2 are highlighted in Table 4 for all the thin film samples. The non-linear refractive index increased with the increase in linear refractive index. This is owing to a high polarizability reliance on molecules and the distortion of the density of electrons in the electric field [39].

It has been found that the linear and nonlinear optical parameters $\chi^{(1)}$, $\chi^{(3)}$, and n_2 declined their values after an increase in Ni interlayer concentration and the thickness of designed thin films. It may be owing to a big number density of free charge carriers in the polarized substance. These values are equivalent to the results of varied systems taken by Tichy and Ticha [38], thus, the projected structure of ALD deposited different multilayer thin films of the ZnO/Ni/ZnO here have closely equivalent computed values of $\chi^{(3)}$ and n_2. This highlights their relevance for the utilization of nonlinear optical devices, especially in networks of optical communication that rely primarily on fast-speed signals and fiber optics technology.

3.9. Computation of dielectric constant (ϵ_∞) at the high-frequency limit

To compute the high-frequency dielectric constant, a model was given by Spitzer-Fan [40]. This model enlightens the variation of $n(\lambda)$ based on some consequences viz. the high-frequency lattice dielectric parameter $\boldsymbol{\varepsilon_\infty}$, modes of lattice dynamics, and free-electron charge carriers. Mathematically, the model can be specified by the ensuing relation [40]:

$$n^2 = \varepsilon_\infty - \frac{Ne^2}{4\pi^2\varepsilon_0 m^* c^2}\lambda^2 \tag{25}$$

where e and c denote the electronic charge and the speed of light in a free space whilst N and m^* depict to number density and effective mass of the charge carriers respectively.

A graphical representation for the n^2 as a function of λ^2 produced the linear profiles at a longer wavelength, however, its linearity drops

Table 4
The computed values of linear and nonlinear optical parameters for the ALD deposited different multilayer thin films of the ZnO/Ni/ZnO system.

Sample	Linear and Nonlinear Optical Parameters			$(\epsilon_\infty)_2$	N/m^* ($m^{-3}kg^{-1}$)	ω_p (Hz)
	$\chi^{(3)}$ (esu)	n_2	$\chi^{(1)}$			
$ZN_{10}Z$	8.45×10^{-13}	1.20×10^{-10}	107.16	6.95	2.45×10^{56}	3.2×10^{14}
$ZN_{30}Z$	3.41×10^{-13}	5.30×10^{-11}	43.28	6.59	1.23×10^{57}	7.3×10^{14}
$ZN_{50}Z$	1.90×10^{-13}	5.14×10^{-11}	24.04	5.67	7.36×10^{56}	6.1×10^{14}
$ZN_{70}Z$	1.07×10^{-13}	1.87×10^{-11}	13.50	5.03	1.23×10^{56}	2.7×10^{14}

relatively at a smaller wavelength side for which an anomalous dispersion character is revealed by the index of refraction [refer Fig. 14]. The values of N/m^* and $(\varepsilon_\infty)_2$ were estimated for all the present thin film samples through the gradient and the extrapolation of these plots close to $\lambda = 0$ respectively. The estimated numerical values of N/m^* and $(\varepsilon_\infty)_2$ for all the samples are noted in Table 4.

Further for the calculation of plasma frequency, ω_p, the classical Drude model is used. This model connects the plasma frequency ω_p to the dielectric constant ε_L and the ratio N/m^* of a dielectric material by the subsequent relation [19]:

$$\omega_p = \sqrt{\left(\frac{N}{m^*}\right)\frac{e^2}{\varepsilon_0 \varepsilon_L}} \tag{26}$$

The above relation for the calculation of ω_p is utilized when the resonance of vibrations of free charge carriers is achieved. If the frequencies of incident electromagnetic radiation are high in comparison to the ω_p, the radiation transmits the material whilst it suffers the reflection for the frequencies lower than the ω_p. Calculated values of plasma frequency (ω_p) for the present thin film samples are recorded in Table 4.

On the low-frequency side, the damping constant is lower than the dielectric constant (i.e., electron damping becomes poor). This can be leveled by the ensuing relationship that occurs between the real part of the dielectric constant and the plasma frequency (ω_p) [19]:

$$\varepsilon' = \varepsilon_\infty - \frac{\omega_p^2}{\omega^2} \tag{27}$$

Accordingly, the plotting of the graphs of ε' as a function of ω^{-2} for all the proposed ALD deposited tri-layer thin film samples of ZNZ. The graphical illustration of ε' with $1/\omega^2$ for all the thin films are shown in Fig. 15. Through graphs, the value of $(\varepsilon_\infty)_3$ is calculated from the intercept at $1/\omega^2 = 0$ and plasma frequency is determined from the slope of the graphs.Add on, the results of $(\varepsilon_\infty)_3$ and ω_p are evaluated and mentioned in Table 5 and Table 4. The evaluated values of ω_p from the Eq. (25) and those from the slopes of the last plots of ε' against ω^{-2}, were also revealed somewhat good matching values. In addition, the results of ω_p for the proposed system are consistent with those of other systems testified elsewhere [41].

It can be observed that the calculated values of the high-frequency dielectric constant recorded in Tables 3 to 5 and labeled by $(\varepsilon_\infty)_1$, $(\varepsilon_\infty)_2$, and $(\varepsilon_\infty)_3$ through three dissimilar methods for ALD deposited tri-layer thin film system considered under the present work, are closely in good agreement. In the computation of the values of $(\varepsilon_\infty)_1$, $(\varepsilon_\infty)_2$, and $(\varepsilon_\infty)_3$, a good match is attained among these values because there is a big difference in the lattice vibration which executes at the plasma frequencies and that happens for the absorption frequency at the band edge. The optical properties of the deposited layered materials were such that both necessities were fulfilled in maximum illustrations [42] and like outcomes were also obtained in this present work. It is also interesting to remark that the values of $(\varepsilon_\infty)_1$, $(\varepsilon_\infty)_2$, and $(\varepsilon_\infty)_3$ are closely well matched that of the high-frequency dielectric constant ε_∞^{WDD} estimated from the WDD approach. The more possible basis for such nice matched values for high-frequency dielectric constant is that the lattice dynamics and restricted carriers in a vacant lattice recline in the translucent region of the optical spectrum [43,44].

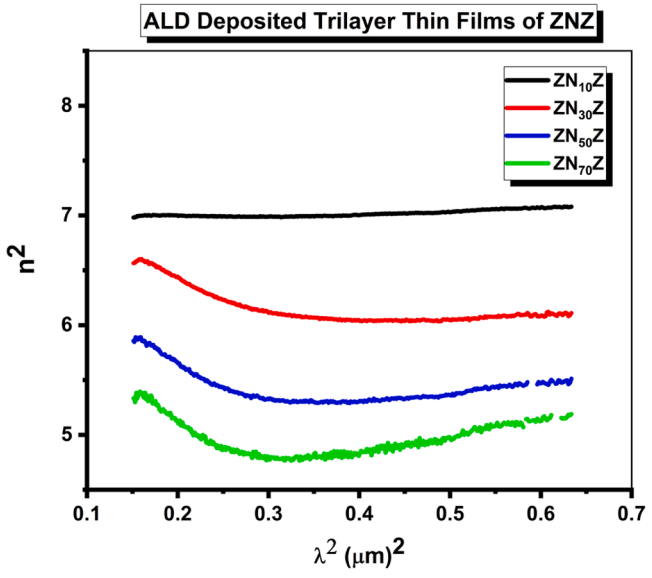

Fig. 14. : A graphical representation of n^2 against λ^2 for ALD deposited different multilayer thin films of the ZnO/Ni/ZnO system.

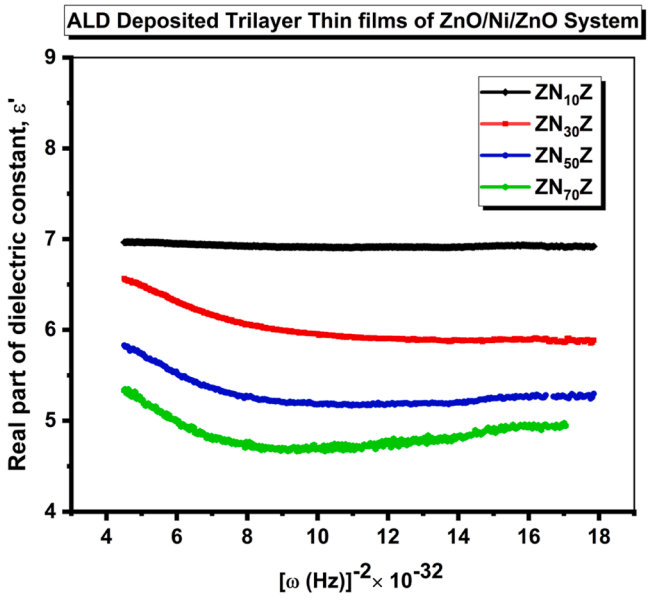

Fig. 15. : A graphical representation of ε' against ω^{-2} for ALD deposited different multilayer thin films of the ZnO/Ni/ZnO system.

Table 5
The computed values of different optical parameters [Charge carriers concentration (N), Relaxation time (τ), high-frequency lattice dielectric parameter $(\varepsilon_\infty)_3$, plasma frequency (ω_p), optical mobility (μ_{opt}), and optical resistivity (ρ_{opt}), high-frequency dielectric constant $(\varepsilon_\infty)_3$, and optical electronegativity (η_{opt})] for the ALD deposited different multilayer thin films of the ZnO/Ni/ZnO system.

Sample	$N(m^{-3})$	τ (sec)	μ_{opt} (C-sec/kg)	ρ_{opt}	$(\varepsilon_\infty)_3$	η_{opt}
$ZN_{10}Z$	9.83 × 10^{25}	8.03 × 10^{-17}	3.21× 10^{-5}	1.99 × 10^{-3}	6.96	1.76
$ZN_{30}Z$	4.91 × 10^{26}	3.47 × 10^{-16}	1.39 × 10^{-4}	9.16 × 10^{-5}	6.52	1.78
$ZN_{50}Z$	2.95 × 10^{26}	2.33 × 10^{-16}	9.32 × 10^{-5}	2.28 × 10^{-4}	5.64	1.81
$ZN_{70}Z$	4.91 × 10^{25}	4.38 × 10^{-17}	1.75 × 10^{-5}	7.25 × 10^{-3}	4.99	1.84

3.10. Computation and study of the complex dielectric constant close to the absorption edge

To determine the real part of the electronic dielectric constant, ε' and the imaginary part of the electronic dielectric constant ε'' for the present ALD deposited thin film system of ZNZ, the ensuing relations are utilized [45]:

$$\varepsilon = \varepsilon' + i\varepsilon'' \tag{28a}$$

$$\varepsilon = (n + ik)^2 \tag{28b}$$

After solving above mentioned two equations the forms for ε' and ε'' are thus, defined by the following equations:

$$\varepsilon' = n^2 - k^2 \tag{28c}$$

and

$$\varepsilon'' = 2nk \tag{28d}$$

The graphical depiction for ε' and ε'' as a function of energy, $h\nu$ are shown in Fig. 16 and Fig. 17 for the present proposed ALD deposited thin film system.

3.11. Analysis of the dissipation factor tanδ

To get more information about the present materials from the optical characteristics, one very stimulating optical quantity is loss tangent tanδ. The loss tangent signifies the amount of loss in power taking into account the mechanical oscillator which is present in the dissipative structure. It is usually observed that dielectric substances dissipate electric power mostly via heating. Therefore, the dissipation or lass factor can be defined by the subsequent equation [19]:

$$\tan\delta = \frac{\varepsilon''}{\varepsilon'} \tag{29}$$

The variation in tan δ as a function of the energy of incident radiation for the present proposed thin film system is revealed in Fig. 18. The value of tan δ substantially decreases with increasing the energy of the incident radiation for all the deposited multilayer thin films of the ZnO/Ni/ZnO system. Furthermore, the value of the dissipation or loss factor was found to be increased after changing the thickness of multilayer Ni concentration from 10 to 70 nm in all the deposited thin film samples.

3.12. Computation and analysis of optical σ_{opt} and electrical σ_{ele} conductivities

To observe the optical response of yielded material in terms of its optical conductivity, the frequency of the material can only be specified in Gaussian units. Thus, the optical response in terms of the optical

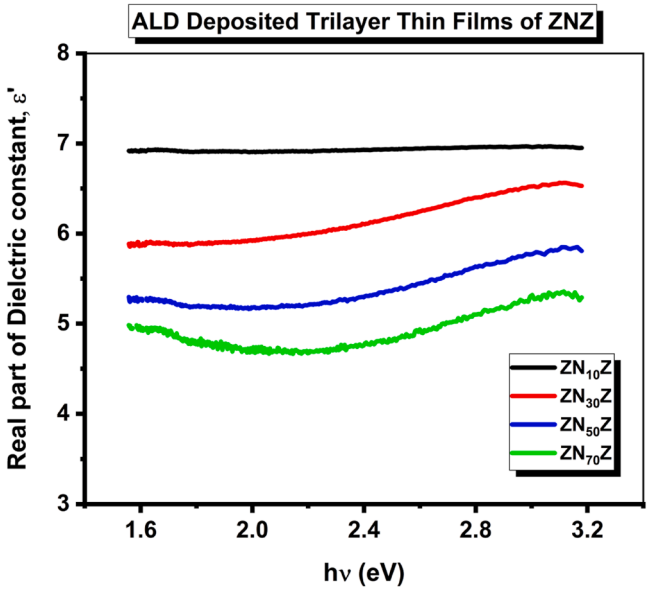

Fig. 16. : An illustration of the real part of dielectric constant ε' as a function of incident photon energy hν for ALD deposited different multilayer thin films of the ZnO/Ni/ZnO system.

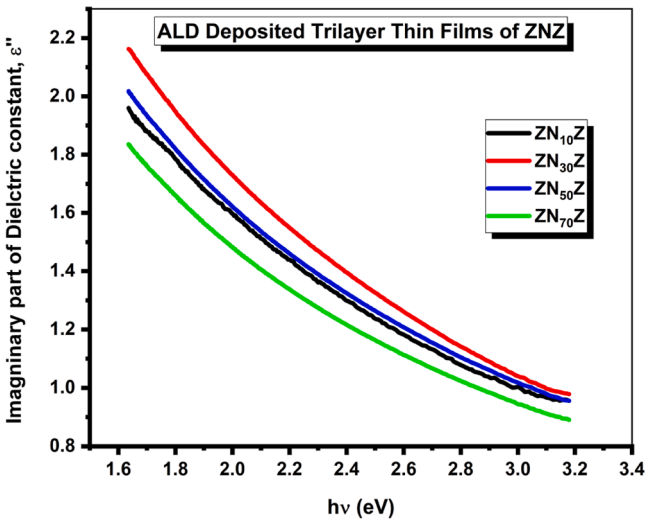

Fig. 17. : An illustration of the imaginary part of dielectric constant ε'' as a function of incident photon energy hν for ALD deposited different multilayer thin films of the ZnO/Ni/ZnO system.

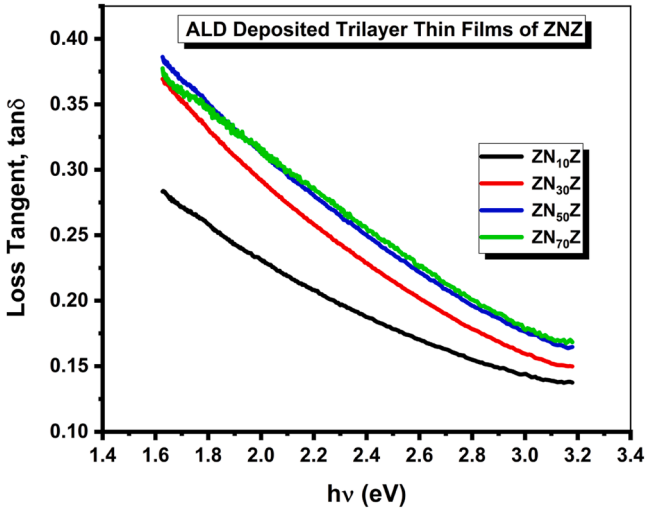

Fig. 18. : An illustration of loss factor tan δ as a function of incident photon energy hν for ALD deposited different multilayer thin films of the ZnO/Ni/ZnO system.

conductivity (σ) can be expressed by the following relation [19]:

$$\sigma_{opt} = \frac{\alpha nc}{4\pi} \tag{30}$$

A graphical representation of optical conductivity (σ_{opt}) as a function of the energy of incident radiation (hν) for all deposited layered samples is shown in Fig. 19. We notice that the optical conductivity consistently varies with α and n of the samples. It follows a similar trend which is followed by α. The value of σ_{opt} decreases with increasing the energy of incident radiation for all the deposited different multilayer thin films of the ZnO/Ni/ZnO system. It can be observed from the plots that the optical conductivity is slightly increased after increasing the interlayer thickness of Ni concentration in different multilayer thin films ZnO/Ni/ZnO system and it attains an optimum change for ZN50Z thin film sample and its value slightly reduced further increasing the interlayer thickness of Ni concentration. Thus, the multilayer thin films of the ZnO/Ni/ZnO system under present work show a good photo-response feature owing to their good optical conductivity results.

Additionally, we have calculated the electrical conductivity results

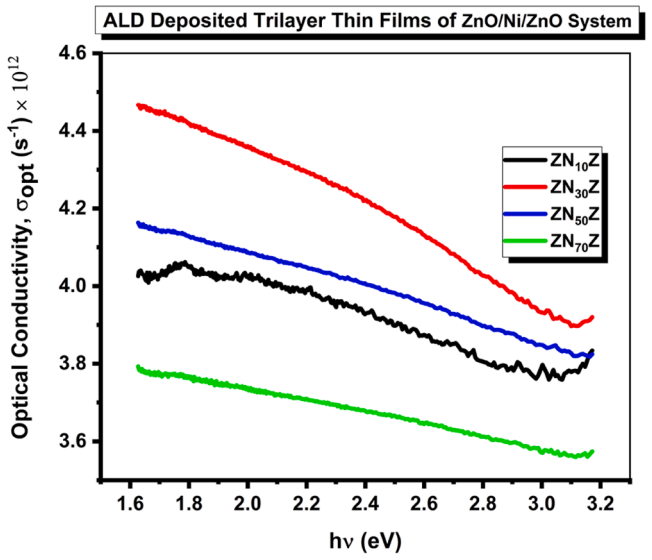

Fig. 19. : A graphical representation of optical conductivity σ_{opt} as a function of incident photon energy hν for ALD deposited different multilayer thin films of the ZnO/Ni/ZnO system.

for the present system by utilizing absorption coefficient α and optical conductivity, σ_{opt} with the help of the following expression [19,46]:

$$\sigma_{ele} = \frac{2\lambda\sigma_{opt}}{\alpha} \tag{31}$$

A graphical depiction of the variation in σ_{ele} as a function of incident radiation energy $h\nu$ for present prepared layered samples is shown in Fig. 20. The value of σ_{el} significantly reduces with the increasing photon energy $h\nu$ of incident radiation for all the deposited different multilayer thin films of the ZnO/Ni/ZnO system. This decreasing trend in σ_{ele} with the increasing photon energy $h\nu$ of incident radiation supports the semiconducting character of the ALD deposited different multilayer thin films ZnO/Ni/ZnO system. From Fig. 20, we can see that the value of electrical conductivity is somewhat decreased as we change the inter-layer thickness of Ni concentration in different multilayer thin films ZnO/Ni/ZnO system and it displays an optimum variation for ZN70Z thin. It may be owing to some structural changes in the matrix of the

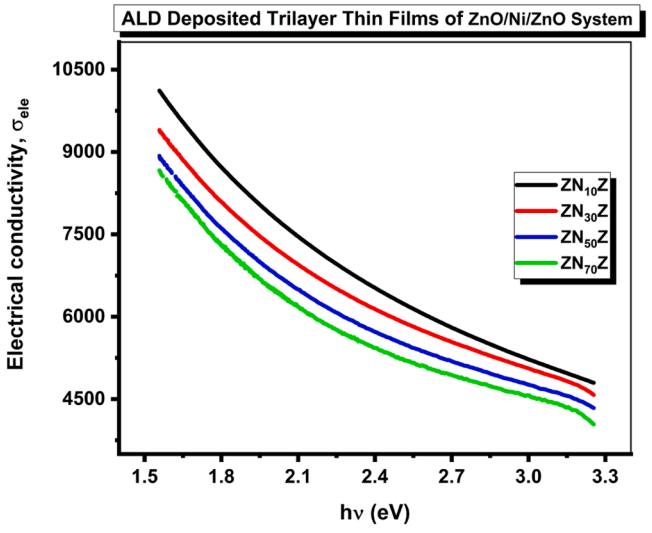

Fig. 20. : A graphical representation of electrical conductivity σ_{ele} as a function of incident photon energy hν for ALD deposited different multilayer thin films of the ZnO/Ni/ZnO system.

different multilayer thin films ZnO/Ni/ZnO system.

3.13. Evaluation of relaxation time, optical mobility, optical resistivity, and optical electronegativity

The classical Drude free-electron theory is very important to evaluate the several optoelectrical constants by scrutinizing them together with the real and imaginary portions of dielectric constants. This theory recommends the wavelength reliant on both real part and imaginary part of dielectric constants that are stated by the previous relation (24) and subsequent relation given as [35,47]:

$$\varepsilon' = \frac{e^2}{4\pi^3\varepsilon_0 c^3}\left[\left(\frac{N}{m^*}\right)\left(\frac{1}{\tau}\right)\right]\lambda^3 \tag{32}$$

In this equation, τ represents the relaxation time. To evaluate the value of relaxation time τ, we have plotted the graph between ε' and λ^3. [see Fig. 21(a)]. As we can see the gradient of the linear plot is equal to $\frac{e^2}{4\pi^3\varepsilon_0 c^3}\left[\left(\frac{N}{m^*}\right)\left(\frac{1}{\tau}\right)\right]$. Thereby the value of τ for the proposed thin film system is computed from the gradient and by utilizing the previously determined result of (N/m^*). Additionally, in the aforementioned relation (32), the calculation of m^* is done by relating m^* with m_0 through an expression- $m^* = 0.44m_0$, hence, the value of N is evaluated for all the thin film samples. The evaluated values of both relaxation time (τ) and the number density (N) of free charge carriers are tabulated in Table 5. The results show that the values of relaxation time lie between 0.04×10^{-15} s and 0.35×10^{-15} for all the thin film samples under the present

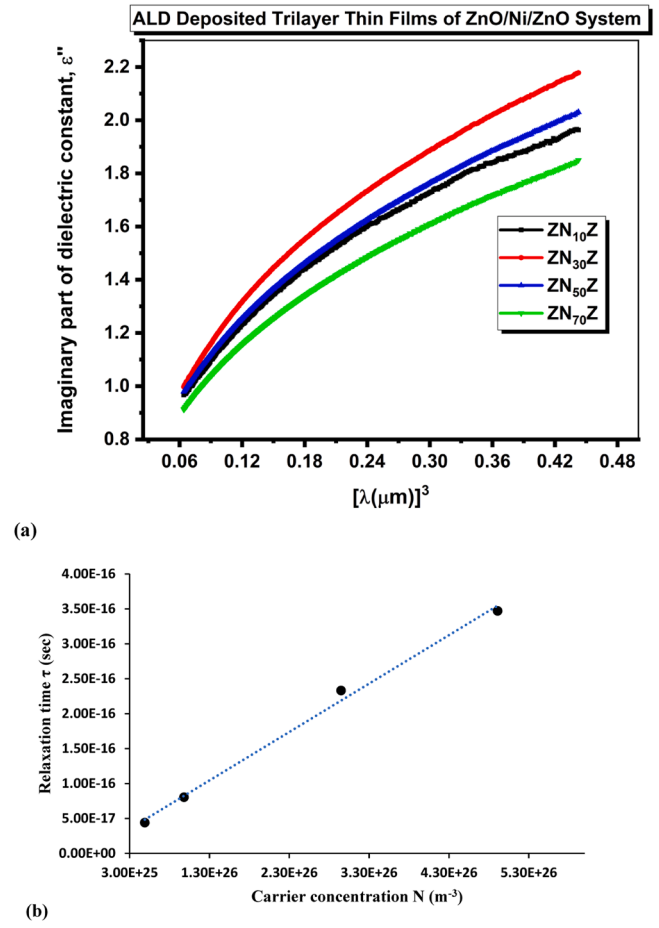

Fig. 21. : (a) A graphical representation of the imaginary part of dielectric constant ε'' against λ^3 for ALD deposited different multilayer thin films of the ZnO/Ni/ZnO system, and (b) variation of the relaxation time with carrier concentration.

work and are consistent with the earlier results [48,49].

The carrier concentration significantly affects the strength of the nonlinear optical response since the carrier lifetime and mobility can affect the strength and temporal characteristics of nonlinear optical phenomena. For instance, the relationship between the carrier concentration with nonlinear characteristics can be understood in terms of the nonlinear optical response since the nonlinear optical characteristics refer to the optical response of a material that is not directly proportional to the intensity of the incident light. Nonlinear optical effects often arise due to the interaction of light with the electronic structure of a material and it is affected with the carrier concentration. The relaxation time of carriers in the present study rises linearly with increasing carrier concentrations which indicates that it is intimately linked to their nonlinear optical characteristics [see Fig. 21(b)]. Nevertheless, the current explanation is primarily qualitative, and at this juncture, it is not possible to disclose precise quantitative information. We anticipate that further studies will eventually identify the precise function of carrier concentration in regulating the nonlinear optical properties.

Additionally, to evaluate the values of optical mobility and resistivity (i.e., μ_{opt} and ρ_{opt}) for all the deposited thin films, setting the calculated values of the parameters N and τ in the following equations [50]:

$$\mu_{opt} = \frac{e\tau}{m^*} \tag{33}$$

and

$$\rho_{opt} = \frac{1}{e\mu_{opt}N} \tag{34a}$$

$$\rho_{opt} = \frac{m^*}{e^2\tau N} \tag{34b}$$

The calculated values of ρ_{opt} and μ_{opt} for the present, all samples are listed in Table 5. The results obtained in the present work are closer to the values of other previously published works [48,50].

As suggested by Duffy [21,51], a few physicochemical properties of materials are described and directly linked by optical electronegativity. It indicates the ability to attract an electron to an atom to make an ionic bond. To obtain info about the optoelectronic structures for different materials, a model was suggested by Duffy [21,51]. Thereby, the optical electronegativity is defined by the following [52]:

$$\eta_{opt} = \left[\frac{F}{n}\right]^{1/4} \tag{35}$$

Here F represents a constant. Its value is equivalent to 25.54 for many materials. For the present thin film system, the estimated value of η_{opt} is tabulated in Table 4. It can be seen from Table 5 that the value of the optical electronegativity is slightly increased with increasing the interlayer thickness of Ni concentration from 10 to 70 nm in different multilayer thin films of the ZnO/Ni/ZnO system and it gets slightly more value for the thin film ZN70Z. The values of optical electronegativity under the present work for the ALD deposited different multilayer thin films of ZnO/Ni/ZnO system are varied between 1.76 and 1.84. These outcomes are approached with a few other layered materials [53,54].

4. Conclusions

The present work shows the successful deposition of ZnO/Ni/ZnO multilayer thin films with diverse Ni interlayer thickness using atomic layer deposition (ALD) and magnetron sputtering. The interlayer thickness of Ni influences significantly the structural and optical properties of ALD-deposited thin films of ZnO/Ni/ZnO. A detailed investigation shows that the direct optical bandgap values are increased as increasing the thickness of inter-layer Ni material from 10 to 70 nm into the multilayer thin films of the ZnO/Ni/ZnO system. The optical bandgap lies between 2.46 eV to 2.99 eV, which led to a shift of the absorption edge along the higher energy sides. A relationship has been noticed between the linear index of refraction value $(\eta_0)$and the optical energy band gap in terms of the metallization criterion, electrical polarizability, and dielectric parameters based on observed and theoretical results. The results revealed that the linear index of refraction is a vital parameter and it is related to the metallization of oxide material. The calculated values of the index of refraction are reduced by changing the interlayer thickness of Nickle concentration from 10 to 70 nm in all the deposited different multilayer thin films of the ZnO/Ni/ZnO system. Further, the single oscillator model given by Wemple and DiDomenico (WDD) is applicable in the present case. The single oscillator energy parameters, dielectric constant, plasma frequency, optical resistivity, optical mobility, optical electronegativity, and other associated linear and nonlinear optical parameters are changed by increasing the interlayer thickness of Ni concentration from 10 to 70 nm in all the deposited multilayer thin films of the ZnO/Ni/ZnO system. The outcomes of the numerous optical parameters can be understood in terms of changes in structural dimensionality in the metal oxide network.

CRediT authorship contribution statement

A. Sharma: Validation, Methodology, Investigation. **Neeraj Mehta:** Writing – review & editing, Methodology. **E. Barádacs:** Formal analysis. **M. Nabil:** Formal analysis. **Z. Erdélyi:** Writing – original draft, Supervision, Resources, Funding acquisition. **S. S. Fouad:** Writing – original draft, Investigation, Conceptualization.

Declaration of Competing Interest

The authors declare that they have no known competing financial interests or personal relationships that could have appeared to influence the work reported in this paper.

Data Availability

Data will be made available on request.

Acknowledgments

The samples used in this study were prepared and the X-ray patterns were measured at the University of Debrecen, Hungary, according to the agreement between the Faculty of Education, Ain Shams University "**Coordinator and Supervisor Prof. Dr. Suzan Fouad"** and the Faculty of Science and Technology, the University of Debrecen**" Coordinator and Supervisor Prof. Dr. Zoltán Erdélyi".** The optical parameters were measured at the central lab of the physics department at the Faculty of Education at Ain Shams University. This work (project no. TKP2021-NKTA-34) has been implemented with the support provided by the National Research, development, and Innovation Fund of Hungary, financed under the TKP2021-NKTA funding scheme. One of us, N. Mehta is thankful to his university for providing an incentive grant under the Institutes of Eminence (IOE) scheme (Dev. Scheme No. 6031).

References

[1] H. Zaka, B. Parditka, Z. Erdelyi, H.E. Atyia, P. Sharma, S.S. Fouad, Investigation of dispersion parameters, dielectric properties and opto–electrical parameters of ZnO thin film grown by ALD, Optik 203 (2020) 163933.
[2] S.S. Fouad, M. Nabil, B. Parditka, A.M. Ismail, E. Baradács, H.E. Atyia, Z. Erdelyi, Assessing, surface morphology, optical, and electrical performance of ZnO thin film using ALD technique, J. Nanopart. Res. 25 (2023) 172.
[3] S.S. Fouad, B. Parditka, A.E. Bekheet, H.E. Atyia, Z. Erdelyi, ALD of TiO_2/ZnO mutilayers towards the understanding of optical properties and polarizability, Opt. Laser Tech. 140 (2021) 107035.
[4] R. Sha, A. Basak, P. Maity, S. Badhulika, ZnO nano-structured based devices for chemical and optical sensing applications, Sens. Actuators Rep. 4 (2022) 100098.
[5] J. Huang, Z. Yin, Q. Zheng, Applications of ZnO in organic and hybrid solar cells, Energy Environ. Sci. 4 (2011) 3861–3877.

[6] A. Mauro, M. Fragalá, V. Privitera, G. Impellizzeri, ZnO for application in photocatalysis: From thin films to nanostructures, Mater. Sci. Semicond. Process. 69 (2017) 44–51.
[7] S.S. Fouad, B. Parditka, M. Nabil, E. Baradács, S. Negm, Z. Erdélyi, Effect of Cu interlayer on opto-electrical parameters of ZnO thin films, J. Mater. Sci: Mater. Electron 33 (26) (2022) 20594–20603.
[8] A.J. Kulandaisamy, C. Karthek, P. Shankar, G. Mani, J. Rayappan, Tuning selectivity through cobalt doping in spray pyrolysis deposited ZnO thin films, Ceram. Int. 42 (2016) 1408–1415.
[9] A. Srivastava, Nishant Kumar, S. Khare, Enhancement in UV emission and band gap by Fe doping in ZnO thin films, Opto-Electron. Rev. 22 (2014) 68–76.
[10] N. Kaneva, D. Dimitrov, C. Dushkin, Effect of nickel doping on the photocatalytic activity of ZnO thin films under UV and visible light, Appl. Surf. Sci. 257 (2011) 8113–8120.
[11] S. Ghosh, P. Srivastava, B. Pandey, M. Saurav, P. Bharadwaj, D. Avasthi, D. Kabiraj, S.M. Shivaprasad, Study of ZnO and Ni-doped ZnO synthesized by atom beam sputtering technique, Appl. Phys. A 90 (2008) 765–769.
[12] M. Yilmaz, Characteristic properties of spin coated ZnO thin films: the effect of Ni doping, Phys. Scr. 89 (2014) 095802.
[13] S.K. Avinashi, P. Singh, Shweta, K. Sharma, A. Hussain, D. Singh, C. Gautam, Morphological, mechanical, and biological evolution of pure hydroxyapatite and its composites with titanium carbide for biomedical applications, Ceram. Int. 48 (2022) 18475–18489.
[14] J. Tauc, North-Holland, Amsterdam, Opt. Prop. Solids (1970).
[15] W.E. Vargas, G.A. Niklasson, Applicability conditions of the Kubelka-Munk theory, Appl. Opt. 36 (1997) 5580–5586.
[16] A.K. Zak, A.M. Hashim, M. Darroudi, Optical properties of ZnO/$BaCO_3$ nanocomposites in UV and visible regions, Nanoscale Res. Lett. 9 (2014) 399.
[17] A.P. Indolia, M.S. Gaur, Optical properties of solution grown PVDF-ZnO nanocomposite thin films, Polym. Res. 20 (2013) 43.
[18] D. Bhattacharya, S. Chaudhuri, A.K. Pal, Band gap and Optical Transitions in Thin Films from Reflectance Measurements, Vacuum 43 (4) (1992) 313–316.
[19] J.I. Pankove, Optical Processes in Semiconductors (New York: Dover), 1976.
[20] Springer Handbook of Electronic and Photonic Materials: Fundamentals and Characterization, Safa Kasap, Cyril Koughia, Jai Singh (Eds.), Springer Handbook of Electronic and Photonic Materials, (2007). ISBN: 978-0-387-26059-4.
[21] J.A. Duffy, Trends in energy gaps of binary compounds: an approach based upon electron transfer parameters from optical spectroscopy, J. Phys. C. Solid State Phys. 13 (16) (1980) 2979.
[22] N. Berwal, S. Dhankhar, P. Sharma, R.S. Kundu, R. Punia, N. Kishore, Physical, structural and optical characterization of silicate modified bismuthborate-tellurite glasses, J. Mol. Struct. 1127 (2017) 636–644.
[23] Charles M. Bowden, Mark J. Bloemer, Focus issue: local field effects, Opt. Express 1 (1997), 133-133.
[24] K.F. Herzfeld, On atomic properties which make an element a metal, Phys. Rev. 29 (1927) 701.
[25] B. Pal, D. Sarkar, P.K. Giri, Structural, optical, and magnetic properties of Ni doped ZnO nanoparticles: Correlation of magnetic moment with defect density, Appl. Surf. Sci. 356 (2015) 804–811.
[26] S.B. Rana, R.P.P. Singh, Investigation of structural, optical, magnetic properties and antibacterial activity of Ni-doped zinc oxide nanoparticles, J. Mater. Sci.: Mater. Electron. 27 (2016) 9346–9355.
[27] G. Srinet, R. Kumar, V. Sajal, Structural, optical, vibrational, and magnetic properties of sol-gel derived Ni doped ZnO nanoparticles, J. Appl. Phys. 114 (2013) 033912.
[28] J. Zhao, L. Wang, X. Yan, Y. Yang, Y. Lei, J. Zhou, Y. Huang, Y. Gu, Y. Zhang, Structure and photocatalytic activity of Ni-doped ZnO nanorods, Mater. Res. Bull. 46 (2011) 1207–1210.
[29] S. Agrohiya, S. Dahiya, P. Goyal, I. Rawal, A. Ohlan, R. Poonia, A. Maan, Nickel doped zinc oxide thin films for visible blind ultraviolet photodetection applications, ECS Sens. 1 (2022) 043601.
[30] B. Bhatia, S.L. Meena, V. Parihar, M. Poonia, Optical basicity and polarizability of Nd^{3+}-doped bismuth borate glasses, N. J. Glass Ceram. 5 (2015) 44.
[31] S. Wemple, M. Di-Domenico, Behaviour of the electronic dielectric constant in covalent and ionic materials, Phys. Rev. B 3 (1971) 1338–1351.
[32] S. Wemple, Refractive-index behaviour of amorphous semiconductors and glasses, Phys. Rev. B 7 (1973) 3767–3777.
[33] S.S. Fouad, B. Parditka, A.E. Bekheet, H.E. Atyia, Z. Erdelyi, ALD of TiO_2/ZnO mutilayers towards the understanding of optical properties and polarizability, Opt. Laser Technol. 140 (2021) 107035.
[34] J.N. Zemel, J.D. Jensen, R.B. Schoolar, Electrical and Optical Properties of Epitaxial Films of PbS, Pbse, PbTe, and SnTe, Phys. Rev. A 140 (1965) 330–342.
[35] T.S. Moss, Optical Properties of Semiconductors, Butter Worth's Scientific Publication Ltd, London, 1959.
[36] G. Nagpal, I. Sharma, S. Tripathi, The effect of the substitution of Sb with Zn on the optical and physical properties of $Se_{90}Sb_{10-x}Zn_x$ ($x = 0$, 2, 4, 6, 10 at%) thin films, Opt. -Int. J. Light Electron Opt. 207 (2020) 164460.
[37] S. Fouad, B. Parditka, A. Bekheet, H. Atyia, Z. Erdelyi, ALD of TiO_2/ZnO multilayers towards the understanding of optical properties and polarizability, Opt. Laser Technol. 140 (2021) 107035.
[38] H. Titcha, L. Titchy, Semiempirical relation between non-linear susceptibility (refractive index), linear refractive index and optical gap and its application to amorphous chalcogenides, J. Optoelectron. Adv. Mater. 4 (2002) 381–386.
[39] K. Herzfeld, On Atomic Properties which make an Element a MetalPhys, Rev 29 (1927) 701–705.
[40] W. Spitzer, H. Fan, determination of optical constants and carrier effective mass of semiconductors, Phys. Rev. 106 (1957) 882–890.
[41] G.B. Sakr, I.S. Yahia, M. Fadel, S.S. Fouad, N. Romčević, Optical spectroscopy, optical conductivity, dielectric properties, and new methods for determining the gap states of CuSe thin films, J. Alloy. Compd. 507 (2010) 557–562.
[42] N. Sharma, S. Sharma, A. Sarin, R. Kumar, Effect of Sb addition on linear and non-linear optical properties of amorphous Ge–Se–Sn thin films. Opt. Mater. 51 (2016) 56–61.
[43] H.E. Atyia, Influence of deposition temperature on the structural and optical properties of $InSbSe_3$ films, J. Optoelectron. Adv. Mater. 8 (2006) 1359–1366.
[44] M.M.A. Aziz, E.G.E. Metwally, M. Fadel, H.H. Labib, M.A. Afifi, Optical properties of amorphous Ge-Se-Tl system films, Thin Solid Films 386 (2001) 99–104.
[45] A.M. Abd-Elnaiem, M. Mohamed, R.M. Hassan, A.A. Abu-Sehly, M.A. Abdel-Rahim, M.M. Hafiz, Influence of annealing temperature on the structural and optical properties of $As_{30}Te_{70}$ thin films, Mater. Sci. Pol. 35 (2017) 335–345.
[46] T.C.S. Girisun, S. Dhanuskodi, Linear and nonlinear optical properties of tris thiourea zinc sulphate single crystals, Cryst. Res. Technol. 44 (2009) 1297–1302.
[47] I. Saadeddin, B. Pecquenard, J.P. Manaud, R. Decourt, C. Labrugere, T. Buffeteau, G. Campet, Synthesis and characterization of single- and co-doped SnO_2 thin films for optoelectronic applications, Appl. Surf. Sci. 253 (2007) 5240–5249.
[48] M.S.E. Bana, S.S. Fouad, Opto-electrical characterisation of $As_{33}Se_{67-x}Sn_x$ thin films, J. Alloy. Compd. 695 (2017) 1532–1538.
[49] A.S. Hassanien, Studies on dielectric properties, opto-electrical parameters and electronic polarizability of thermally evaporated amorphous $Cd_{50}S_{50-x}Se_x$ thin films, J. Alloy. Compd. 671 (2016) 566–578.
[50] F. Lai, L. Lin, R. Gai, Y. Lin, Z. Huang, Determination of optical constants and thicknesses of In_2O_3:Sn films from transmittance data, Thin Solid Films 515 (2007) 7387–7392.
[51] M. Duffy, L. Warner, Longman KS3 Test Pack, Pearson Education, 2003.
[52] R. Reddy, K.R. Gopal, K. Narasimhulu, L.S.S. Reddy, K.R. Kumar, C.K. Reddy, S. N. Ahmed, Opt. Mater. 31 (2008) 209–212.
[53] M.S. El-Bana, S.S. Fouad, Opto-electrical characterisation of $As_{33}Se_{67-x}Sn_x$ thin films, J. Alloy. Compd. 695 (2017) 1532–1538.
[54] A.S. Hassanien, Studies on dielectric properties, opto-electrical parameters and electronic polarizability of thermally evaporated amorphous $Cd_{50}S_{50-x}Se_x$ thin films, J. Alloy. Compd. 671 (2016) 566–578.